EXPERIMENTAL AND FEM INVESTIGATION OF SIF IN DCB SPECIMEN

By

KESAVAN POTTY P. K.

ME

1992

M

POT

EXP

DEPARTMENT OF MECHANICAL ENGINEERING

INDIAN INSTITUTE OF TECHNOLOGY KANPUR

APRIL, 1992

EXPERIMENTAL AND FEM INVESTIGATION OF SIF IN DCB SPECIMEN

A Thesis Submitted
in Partial Fulfilment of the Requirements
for the Degree of

MASTER OF TECHNOLOGY

by

KESAVAN POTTY P.K.

to the

DEPARTMENT OF MECHANICAL ENGINEERING
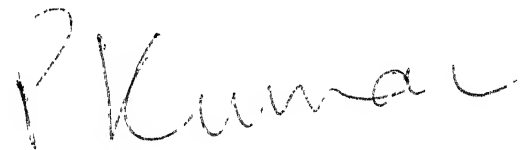
INDIAN INSTITUTE OF TECHNOLOGY KANPUR

April, 1992

CERTIFICATE

It is certified that the work contained in the thesis entitled "EXPERIMENTAL AND FEM INVESTIGATION OF SIF IN DCB SPECIMEN", by "KESAVAN POTTY P. K.", has been carried out under my supervision and that this work has not been submitted elsewhere for a degree.

Dr. Prashant Kumar

Professor

Department of Mechanical Engg.

India Institute of Technology

Kanpur — 208016

April, 1992.

ACKNOWLEDGEMENTS

I am extremely grateful to Dr. Prashant Kumar for his invaluable guidance throughout this work. While looking back, I realize that without his constant encouragements I could not have surmounted the difficulties during the research.

I am equally thankful to Dr. N. N. Kishore for his guidance and encouragement.

I am indebted to Mr. A. K. Yadav and Mr. Abdul Jaleel for their help especially during the numerical work. I thank both for allowing me to use two subroutines in the analysis.

Mr. S. K. Verma deserves special thanks for teaching me to see things the way they are. At times, his pieces of advice have helped me get out of my blues.

I am grateful to Dr. Badri Ray, Mr. S. C. Gupta, Mr. J. Bandyopadhyay and Mr. N. S. Shaktishiromani for all the help and for providing a perfect environment to work in. I am indebted to all my friends in the E.S.A. Lab and Mr. B. K. Jain of Material Testing Lab who continually assisted me in my experimental work. I would like to add a word of appreciation to Mr. R.K. Bajpai of Graphic Arts for the excellent tracings.

I do not claim that the above list is complete, nor do I repudiate any help offered by my other friends who made my sojourn at I.I.T. Kanpur a pleasant one.

- Kesavan Potty P. K.

CONTENTS

LIST OF FIGURES

.

LIST OF TABLES

NOMENCLATURE

a	Crack length
B	Width of the Specimen
C	Compliance of the Cantilever
[D]	Material Property Matrix
E	Young's Modulus
F	Force Acting on surface s
{F}	Force Vector
G	Energy Release Rate
G_{IC}	Critical Energy Release Rate in Mode I
G_{IIC}	Critical Energy Release Rate in Mode II
h	Thickness of each Strip in the DCB Specimen
I	Moment of Inertia
$\lvert J \rvert$	Jacobian
K	Stress Intensity Factor
K_{IC}	Critical Stress Intensity Factor in Mode I
K_{IIC}	Critical Stress Intensity Factor in Mode II
[K]	Stiffness Matrix
P	Load applied to the end of the DCB Specimen
u	Displacement
{u}	Displacement Vector
U	Elastic Strain Energy Stored in the Specimen
W_{ext}	Work supplied by External Force
Φ	Potential Energy of the System
ν	Poisson's Ratio
ε	Strain at a point
σ	Stess at a point
ξ, η	Natural Coordinates

ABSTRACT

Stress intensity factor (K_{IC}) in a double cantilever beam with thin cantilevers is determined through a combined scheme of measuring strain near the crack tip and analysing data by using an FEM programme. The DCB specimen is made from two thin steel cantilevers bonded together with epoxy. The precrack is introduced during bonding by inserting a thin film of BOPP.

The strain field of DCB specimen with thin cantilever cannot be expressed through a closed form solution because the free surfaces are close to the crack plane. Therefore, a finite element software has been developed for finding strain field around the crack tip for a stress intensity factor. This facilitates determination of K_{IC} if strain close to crack tip is measured experimentally by establishing a relationship between strain and stress intensity factor. This relationship is worked out by running the finite element code whenever the crack length is change. The finite element analysis also helps in selecting proper location for strain measurement.

The specimen is loaded in mode I quasi-statically on an INSTRON machine under displacement controlled conditions. The strain is measured through a very small strain gauge of 0.2 mm gauge length, bonded at an angle of 45° to the crack plane. As the crack grows and approaches the strain gauge, the output from the strain gauge increases till it reaches a peak. The peak corresponds to the location of the crack at about 1.5 mm prior to the strain gauge, measured along the crack plane. Further crack extension reduces the strain. The measured peak strain gives the value of critical stress intensity factor through the already established relationship between strain and SIF. The experimentally obtained value of K_{IC} has been compared with numerical values obtained through finite element analysis. The measured value of K_{IC} is found to be lower. The reason is thought to be imperfect bonding between the cantilevers due to air entrapment.

CHAPTER I

INTRODUCTION

In composite materials, one of the major concerns is the poor interlaminar toughness on impact. Under impact loading the interlaminar cracks can propagate at high velocities exceeding 300 m/s, according to observations made using high speed cameras [1]. The problem to be investigated is the relationship between fracture toughness and the crack velocity. This information plays an important role in improving the performance of composite materials. The toughness of interlaminar crack growth may be measured in terms of Critical Energy Release rate (G_{IC} and G_{IIC}) or Critical Stress Intensity Factor (K_{IC} and K_{IIC}).

1.1 MEASUREMENT OF G_{IC} AND G_{IIC}

The method of energy balance applied in the measurement of dynamic G_I or G_{II} is inaccurate as it is not always possible to account for all the energy losses since dynamic experiments deal with wave propagation inside the specimen. As wave propagates, it interacts with defects causing transformation of kinetic and strain energy into heat. Such transformation of energy is also known as deformation friction [2]. The heat produced may increase the temperature of the specimen or part of it may be transferred to the specimen holder or surrounding air. As this heat generation cannot be measured accurately, it affects the results substantially since G for interlaminar fracture in composites is very small, of the order of 200 J/m^2, compared to metals where G is more than 30,000 J/m^2. Hence, we find that experimental determination of dynamic G_{IC} or G_{IIC} is difficult and the stress approach is more suitable.

1.2 MEASUREMENT OF K_{IC} OR K_{IIC}

For specimens with thickness of the order of uncracked ligament, equations are available for calculating stress/strain field in the specimen through the stress intensity factor. But for very thin specimens no such closed form solutions are available in the literature to the best of author's knowledge. Since in the current analysis we are using thin laminate, free lateral surfaces are close to the crack tip (<3 mm thick) and stress or strain fields cannot be predicted by conventional formulae. Moreover, wave propagation effects become prominent under dynamic conditions. So the measurement of K is not straightforward here.

The strategy adopted is to solve the problem in stages. In the first stage, a double cantilever beam (DCB) specimen made of thin isotropic metal (steel) strips bonded with epoxy will be tested for fracture toughness. Assisted by finite element analysis, a proper location will be selected for fixing a small strain gauge to measure the strain near the crack tip in mode I under quasi-static conditions. Based on the results of the finite element analysis, a relationship also will be established between strain and stress intensity factor. A strain gauge of 0.2 mm gauge length will be bonded at the location and the DCB specimen will be loaded in mode I. The measured strain will give the value of K_I through the relationship established between the two. In the second stage, following the same line, use of strain gauges on isotropic materials under dynamic conditions will be investigated. Finally in the third stage, with enough confidence derived from the above two stages, strain gauges will be used on fibre composite materials in dynamic experiments. In this study, work has been done only on the first stage.

1.3 LITERATURE SURVEY

Work on stress/strain field in a double cantilever beam with thin cantilevers loaded statically has not been so far reported in the literature to the best of author's knowledge. However, expression for K_{IC} of such a specimen is listed in [8]. This is derived in an indirect way by first finding compliance, C, of the specimen and then finding G by the formula $G = \frac{1}{2} \frac{P^2}{B} \frac{\partial C}{\partial a}$ where P is the load on the cantilever, a is the crack length and B is the width of the specimen. K_I is then determined by using the formula $K_I = \sqrt{G_I E / (1-\nu^2)}$. The proof is given in Appendix B. In the derivation only flexural energy of the cantilever has been accounted for; that is , the shear strain energy caused by the lateral loads at the cantilevers and the strain energy in the bulk material beyond the crack tip have not been considered in evaluating the compliance. However, the assumption of neglecting these strain energies is reasonable because the cantilevers are thin and flexural energy dominates. Another point to be noted is that the procedure only provides the value of K_I but gives no idea of strain field around the crack tip which is strongly influenced by the nearby traction free surfaces (Sec 2.8.1).

Since work on stress/strain field in DCB specimen is not available in literature, this survey on literature is presented on two related fields viz., (i) stress field around a crack tip in a large FRP plate and (ii) experimental evaluation of dynamic K_I in large metal or plastic plates.

Rosakis, Duffy and Freund [3] performed dynamic crack propagation experiments using wedge loaded double cantilever beam specimens of an austenitized, quenched and tempered 4340 steel. They measured the dynamic stress intensity factor by means of the optical method of caustics. The experimental data was obtained from the shadow spot patterns photographed with a Cranz-Schardin high speed camera. The interpretation of the data was based on an elastodynamic analysis. They obtained the

instantaneous value of the dynamic stress intensity factor K_I^d as a function of crack tip velocity. It is observed that the fracture toughness increases with increase in crack velocity. The specimen used by them was large in size and therefore the technique cannot be used for DCB specimen with thin cantilevers.

Stress Intensity Factor of a crack in a large orthotropic composite materials was measured using strain gauges by Shukla, Agarwal and Bharat Bhushan [4]. They first developed theoretical equations for the strain field in the vicinity of the crack tip in an orthotropic material. These equations were then critically evaluated to obtain the optimum location and orientation of the strain gauges to be used for strain measurements. They then verified the applicability of the procedure using a glass epoxy specimen. This work deals with large plate only and that too under quasi-static loading conditions.

Strain gauges were used by Berger and Dally to measure the dynamic fracture toughness of steel [5]. They recorded a sequence of strain time traces during the passage of crack beneath a line of strain gauges. The data analysis uses the spatial distribution of strains along the gauge line at a specified time. They developed an overdetermined system of equations which are solved to determine K_{ID} as a function of time and position during crack propagation. In this study also, only large plates are dealt with.

Nishioka et. al. [6] studied the specimen size effects on dynamic crack propagation and arrest in DCB specimens using laser caustic method. They worked on polymethyl methacrylate (PMMA) made specimens in mode I. Dynamic condition was obtained using the conventional technique of storing energy through a blunt crack. They worked with maximum crack velocities of the order of 200 m/s. The specimen length was changed in order to study the specimen size effects on dynamic crack propagation and arrest. They found that dynamic stress intensity factor decreases as the

crack moves forward. They also observed that K_{ID} increases with crack velocity. However the studies were conducted on large specimens.

Kolednik in his theoretical study [7] gave a physical interpretation of the J-R curves for elastic-plastic fracture. He derived the difference between the crack-initiation toughness and crack-growth toughness using energy balance under quasi-static conditions. He considered three point bend specimens each of which consists of two parts glued together along the ligament. Here also large specimens were analyzed.

1.4 WORK DONE IN THIS STUDY

A DCB specimen has been prepared which simulates the delamination in composite materials, when loaded in mode I. It is made by gluing two thin hardened alloy steel strips together with epoxy. A finite element code has been developed for estimating the strain field near the crack tip in the specimen which was then related with stress intensity factor. The strain estimations have been made use of in selecting a proper position and orientation for fixing the strain gauge. The specimen has been loaded in mode I (Fig. 1.1) under displacement controlled conditions. The strains near the crack tip have been measured. This observation is matched with strain from the finite element programme and the value of K corresponding to the observed strain is obtained.

The finite element formulation is dealt with in chapter II and the experimental technique is detailed in chapter III. The results are discussed in the IV chapter.
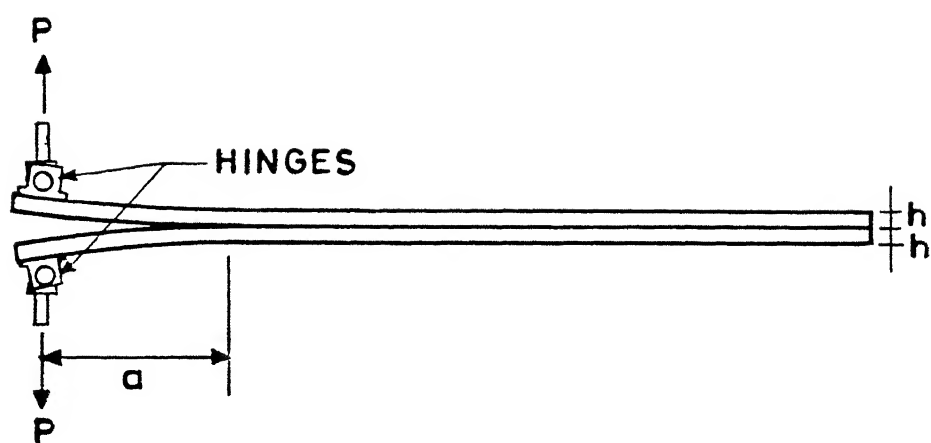
Fig. 1.1   A DCB Specimen.

CHAPTER II

STRAIN FIELD NEAR CRACK TIP OF A DCB
SPECIMEN IN MODE I THROUGH FEM

2.1 INTRODUCTION

In this chapter, numerical analysis has been carried out through FEM to determine the strain field near the crack tip for a double cantilever beam specimen with thin cantilevers, in terms of loads applied at the cantilever ends. The goal of this simulation is to identify a suitable location for a strain gauge near the crack tip so as to optimize its output and relate it to stress intensity factor.

The geometry of the DCB specimen used is shown in Fig. 2.1. It is made by joining two thin strips of hardened alloy steel with epoxy. The epoxy used is LY 556 and the hardener is HY 1907 IN. The curing is done at a temperature of 130 degree Celsius and under a pressure of nearly 4.9 MPa for one hour. The thickness of the epoxy bond is very small, of the order of 0.03mm and is considered to be a line in the numerical formulation. However it is to be noted that the fracture behaviour of the specimen will mostly be determined by the bond.

2.2 SPECIMEN GEOMETRY AND MATERIAL

The alloy steel used is hardened 40Ni2Cr1Mo28[*] (EN 24). Hardening increases its yield stress value thereby decreasing the size of the plastic zone near the crack tip, which is estimated by Irwin's formula [8],

$$r_p = K^2 / \pi \, \sigma_{ys}^2$$

24mm

150 mm

y

20mm

x

2.78 mm

2.78 mm

z

CRACK LENGTH
VARIED BETWEEN
25 and 50 mm
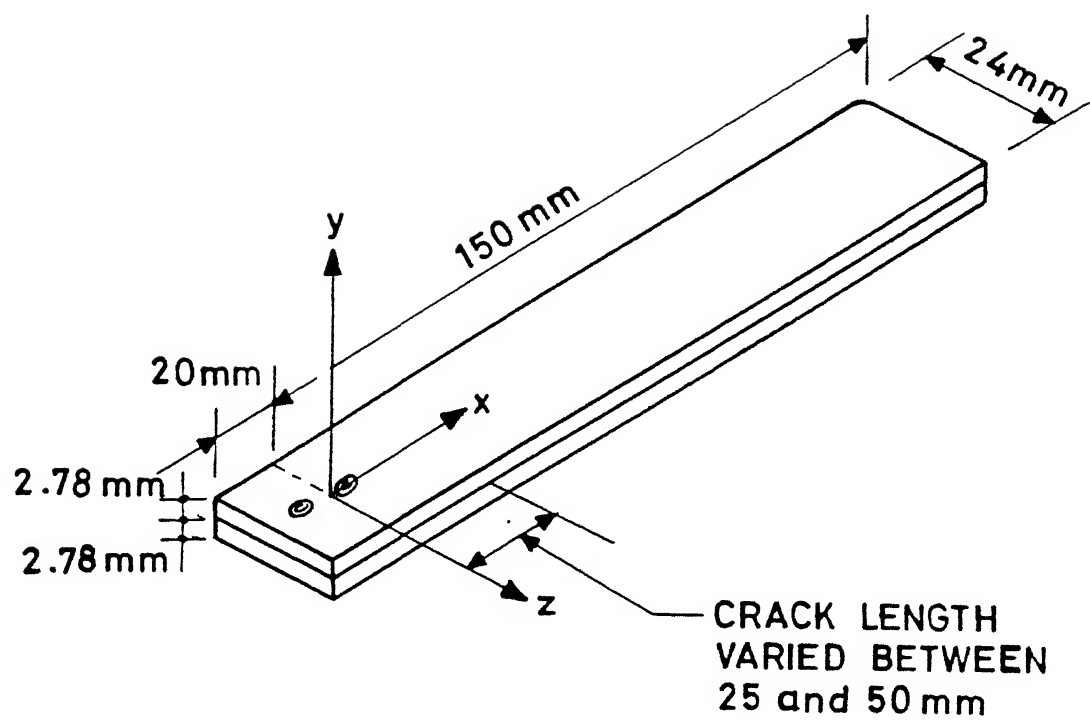
Fig. 2.1   Test Specimen.

In the present case, specimen has a Rockwell hardness of 33 on the C-scale and a yield stress of around 1000 MPa. In order to estimate the size of the plastic zone, K_{Ic} of the DCB specimen was determined through some preliminary experiments by finding G_{Ic} and then using the relation $K_{Ic} = \sqrt{G_{Ic} E} / (1-\nu^2)$ for plane strain. For K_{Ic} of the order of 1.5 MPa$\sqrt{m}$, the plastic zone size is less than 0.0007mm which is small enough to be neglected and the whole region can be considered to be elastic.

2.3 FORMULATION

In this 2-D finite element formulation, the standard method of displacement based stiffness formulation is used [9]. The technique is widely used but for the sake of completeness, it is briefly explained below. Since the dimension along the third direction (Z-direction of Fig. 2.1) is large and since the hinges used to apply load distributes the load uniformly in the Z-direction (Fig. 1.1), this is a plane strain problem.

The objective is to discretize the domain into a number of finite elements, assume a displacement variation in each, construct the potential energy Φ and minimize Φ of the whole body. The potential energy is defined as

$$\Phi = U - W_{ext} \qquad \ldots (2.1)$$

where U represents the strain energy and W_{ext}, the work done by external forces. External forces include boundary forces and body forces. In the present analysis, body forces have been neglected.

For a linear elastic material, the strain energy per unit volume is given as

$$dU = \int_{o}^{\varepsilon_{ij}} \sigma_{ij} d\varepsilon_{ij} = \frac{1}{2} \sigma_{ij} \varepsilon_{ij} \qquad \ldots (2.2)$$

where σ_{ij} and ε_{ij} are stress and strain components at a point within the element.

Thus, the strain energy of the element in a plane problem becomes,

$$\Phi_e = \frac{1}{2} \int \sigma_{ij}\,\varepsilon_{ij}\ dV = \frac{1}{2}\int \left[\ \sigma_{xx}\varepsilon_{xx} + \sigma_{yy}\varepsilon_{yy} + \tau_{xy}\gamma_{xy}\ \right]\ dV$$

Using the matrix notations for stress and strain components,

$$\{\sigma\} = \left\{ \begin{array}{c} \sigma_{xx} \\ \sigma_{yy} \\ \tau_{xy} \end{array} \right\} \qquad \ldots (2.3)$$

$$\{\varepsilon\} = \left\{ \begin{array}{c} \varepsilon_{xx} \\ \varepsilon_{yy} \\ \gamma_{xy} \end{array} \right\} \qquad \ldots (2.4)$$

The strain energy can be expressed in the form,

$$\{\Phi\}_e = \frac{1}{2} \int_v \{\varepsilon\}^T \{\sigma\}\ dV \qquad \ldots (2.5)$$

where v represents the volume of an element.
Work done by surface forces is

$$W_{ext} = \int_s F\ u\ dS \qquad \ldots (2.6)$$

where u is the displacement, F is the force and s is the surface on which F acts. For the 8-noded isoparametric element chosen (Fig. 2.2), the displacements are given by

$$u^x = a_0 + a_1 x + a_2 y + a_3 x^2 + a_4 xy + a_5 y^2 + a_6 x^2 y + a_7 xy^2$$
$$u^y = b_0 + b_1 x + b_2 y + b_3 x^2 + b_4 xy + b_5 y^2 + b_6 x^2 y + b_7 xy^2$$

$$\ldots (2.7)$$
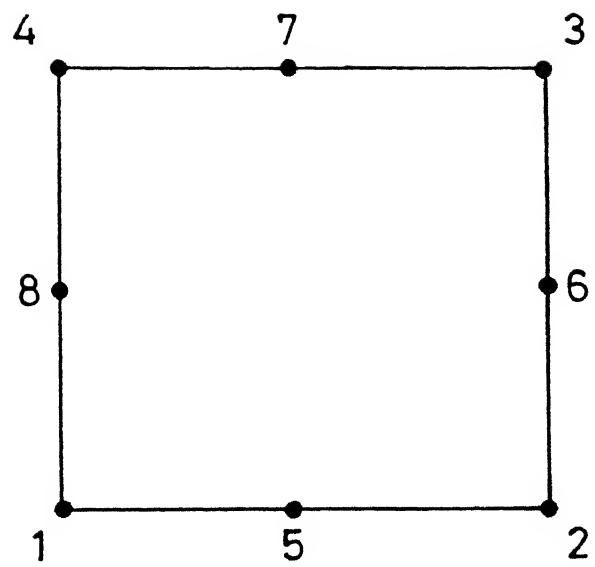
Fig. 2.2   8 Noded Isoparametric Element

where

u^x_1 , u^y_1 at point (x_1, y_1)

u^x_2 , u^y_2 at point (x_2, y_2)

.
.
.

u^x_8 , u^y_8 at point (x_8, y_8)

Alternatively, u^x, u^y can be expressed in terms of nodal displacements in the form

$$\left. \begin{array}{l} u^x = N_1 u^x_1 + N_2 u^x_2 + \quad \ldots \quad + N_8 u^x_8 = \sum N_\iota \, u^x_\iota \\ u^y = N_1 u^y_1 + N_2 u^y_2 + \quad \ldots \quad + N_8 u^y_8 = \sum N_\iota \, u^y_\iota \end{array} \right\} \qquad \ldots (2.8)$$

The geometry mapping can be similarly given as

$$\left. \begin{array}{l} x = \sum N_\iota \, x_\iota \\ y = \sum N_\iota \, y_\iota \end{array} \right\} \qquad \ldots (2.9)$$

where N_1, N_2 etc. are functions of $x, y, x_1, y_1, x_2, y_2, \ldots, x_8, y_8$.
Putting the above two equations into matrix form,

$$\left\{ \begin{array}{c} u^x \\ u^y \end{array} \right\} = \left\{ \begin{array}{cccccccc} N_1 & 0 & N_2 & 0 & \ldots\ldots\ldots\ldots & N_8 & 0 \\ 0 & N_1 & 0 & N_2 & \ldots\ldots\ldots\ldots & 0 & N_8 \end{array} \right\} \left[\begin{array}{c} u^x_1 \\ u^y_1 \\ u^x_2 \\ u^y_2 \\ \vdots \\ u^x_8 \\ u^y_8 \end{array} \right] = [N] \, \{u\}$$

$$\ldots (2.10)$$

The strains can be obtained by differentiating the displacements as

$$
\left\{
\begin{array}{c}
\varepsilon_{xx} \\
\varepsilon_{yy} \\
\gamma_{xy}
\end{array}
\right\}
=
\left\{
\begin{array}{c}
\dfrac{\partial u^x}{\partial x} \\
\dfrac{\partial u^y}{\partial y} \\
\dfrac{\partial u^x}{\partial y} + \dfrac{\partial u^y}{\partial x}
\end{array}
\right\}
$$

which can be further expressed as,

$$
\left\{
\begin{array}{c}
\varepsilon_{xx} \\
\varepsilon_{yy} \\
\gamma_{xy}
\end{array}
\right\}
=
\begin{bmatrix}
\dfrac{\partial N_1}{\partial x} & 0 & \dfrac{\partial N_2}{\partial x} & 0 & \cdots\cdots & 0 \\
0 & \dfrac{\partial N_1}{\partial y} & 0 & \dfrac{\partial N_2}{\partial y} & \cdots\cdots & \dfrac{\partial N_8}{\partial y} \\
\dfrac{\partial N_1}{\partial y} & \dfrac{\partial N_1}{\partial x} & \dfrac{\partial N_2}{\partial y} & \dfrac{\partial N_2}{\partial x} & \cdots\cdots & \dfrac{\partial N_8}{\partial x}
\end{bmatrix}
\left\{
\begin{array}{c}
u^x_1 \\
u^y_1 \\
u^x_2 \\
\vdots \\
u^y_8
\end{array}
\right\}
= [B]\{u\}
$$

$$\ldots (2.11)$$

The stress strain relation is represented as

$$\{\sigma\} = [D]\{\varepsilon\}$$

where [D] is the material property matrix defined as

$$
[D] = \dfrac{E}{(1+\nu)\,(1-2\nu)}
\begin{bmatrix}
1-\nu & \nu & 0 \\
\nu & 1-\nu & 0 \\
0 & 0 & \dfrac{1-2\nu}{2}
\end{bmatrix}
\quad \text{for plane strain.}
$$

In the above matrix, ν is the Poisson's ratio and E is the Young's modulus. Now, the expression for strain energy can be rewritten in the form,

$$U = \tfrac{1}{2} \int_V \{\varepsilon\}^T [\sigma]\, dV = \tfrac{1}{2} \int_A \{u\}^T [B]^T [D][B]\{u\} t\, dxdy \qquad \ldots (2.12)$$

where t is the thickness of the element. Transforming into natural coordinates ξ and η,

$$= \frac{1}{2} \int_A \{u\}^T [B]^T [D][B]\{u\} t |J| \, d\xi d\eta \qquad \ldots (2.13)$$

where $|J|$ is the Jacobian. Substituting in Eq.2.1,

$$\Phi^e = \frac{1}{2} \int_A \{u\}^T [B]^T [D][B]\{u\} t \ |J| \, d\xi d\eta - \int_S F \ u \quad dS$$

$$= \frac{1}{2} \{u\}^T [K^e]\{u\} - \{u\}^T \{F^e\} \qquad \ldots (2.14)$$

where

$$[K] = \int_A [B]^T [D][B] \ |J| \, d\xi \ d\eta$$

and the superscript e represents an element. The total potential energy of the system can be obtained by adding up elemental potential energies.

$$\Phi = \sum_{e=1}^{N} \Phi^e = \sum_{e=1}^{N} \{u\}^T [K^e] \ \{u\} - \sum_{e=1}^{N} \{u\}^T \ \{F^e\}$$

$$= \{u^G\}^T [K^G] \ \{u^G\} - \{u^G\}^T \{F^G\} \qquad \ldots (2.15)$$

Where the superscript G denotes the global domain. It is to be noted here that $K^G = \sum_{e=1}^{N} K^e$ represents assembly and not direct addition.

To find the displacement u which minimizes Φ, $\frac{\partial \Phi}{\partial u}$ is equated to zero. From equation 2.3,

$$\frac{\partial \Phi}{\partial u} = [\bar{K}]^G \{u^G\} - \{F^G\} = 0$$

i.e., $[\bar{K}]^G \{u^G\} = \{F^G\}$ $\qquad \ldots (2.16)$

The set of simultaneous equations $[K]\{u\} = \{F\}$ has been solved using a Sky-line solution algorithm.

In the analysis, the load is applied at the end of the cantilevers so that opening mode conditions are simulated.

2.4 MESH GENERATION

The mesh used is shown in Fig. 2.3 and 2.4. The former shows the fine and coarse elements used whereas the latter shows the collapsed elements at the crack tip. The elements are 8-noded isoparametric ones. Near the crack tip, elements are kept fine and coarse elements are chosen away from the crack tip where stress variations are small. The size of the small elements which lie near the crack tip is 0.5 mm. The coarse elements have a size of 13 mm.

At the crack tip collapsed quarter point elements are made use of to model the square root singularity. The behaviour of quarter point element is explained in Appendix A. In our analysis collapsed quarter point elements are used which has the said property along all directions towards the singular point [11].

2.5. CALCULATION OF STRESS INTENSITY FACTOR

The stress intensity factor can be determined as follows [9] (Fig. 2.5)

$$ K_I = \frac{2 G}{Q+1} \sqrt{\left(\frac{\pi}{2L} \right)} \left[\left(4 \, v_{B2} - v_{c2} \right) - \left(4 \, v_{B1} - v_{c1} \right) \right] \qquad \ldots (2.17) $$

Where   Q = 3 - 4ν

          G = Shear Modulus

          u = x-displacement at the node point

and   v = y-displacement at the node point
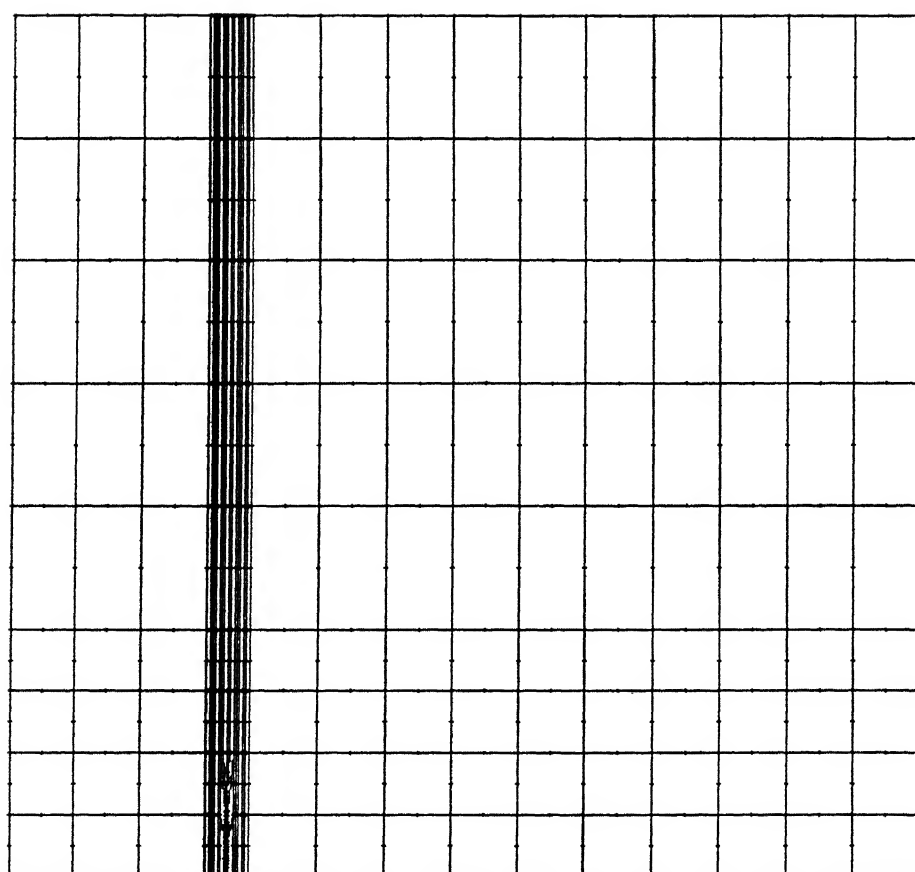
Fig. 2.3   Mesh Showing Coarse and Fine Elements for
DCB Specimen with Thin Cantilevers.
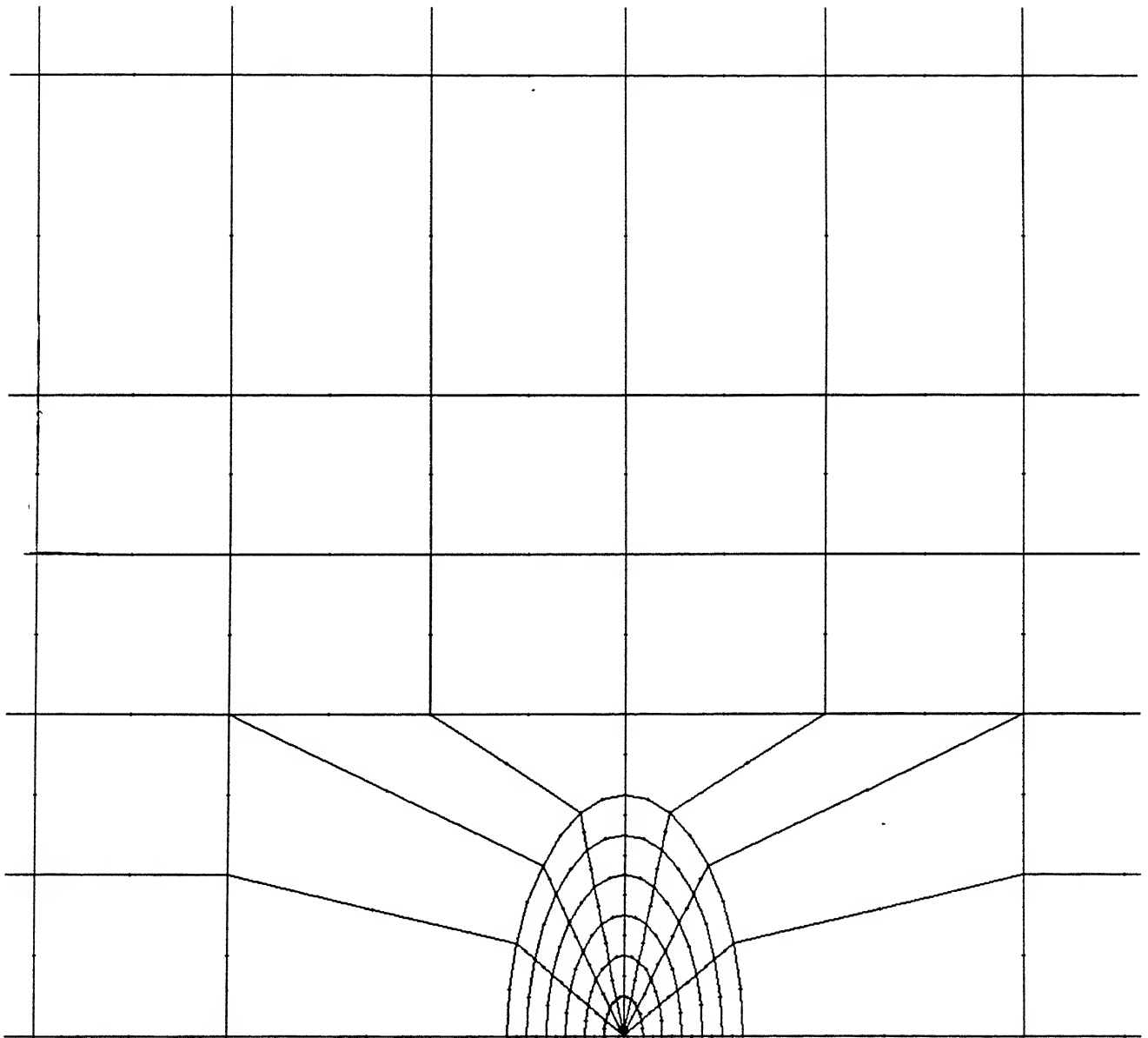
Fig. 2.4   Collapsed Elements at Crack Tip for
DCB Specimen with Thin Cantilevers
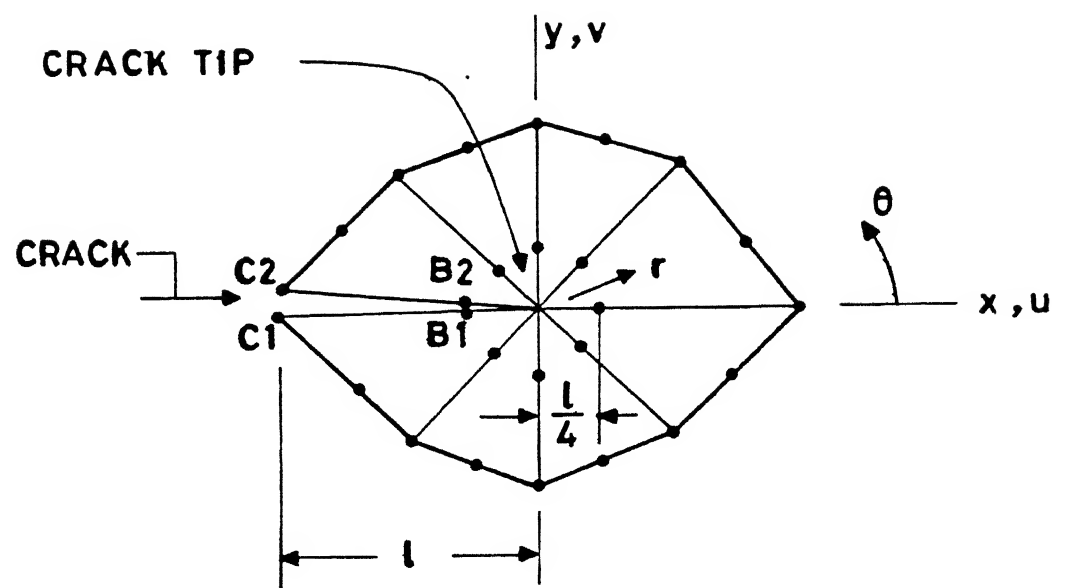
Fig. 2.5 Collapsed Element Near Crack Tip.

2.6 FLOW CHART

The flow chart for the programme is as shown in Fig. 2.6.

```
          ┌──────────────┐
          │    Input     │
          └──────────────┘
                 │
        ┌──────────────────┐                    ┌──────────────┐
        │    Assemble      │────────────────────│  Elemental   │───┌──────────┐
        └──────────────────┘                    │  Stiffness   │   │ Mat Mul  │
                 │                               │   matrix     │   └──────────┘
        ┌──────────────────┐                    └──────────────┘
        │     Apply        │          ┌──────────┐      ┌──────────┐
        │   Boundary       │          │  D mat   │      │  B mat   │
        │  Conditions      │          └──────────┘      └──────────┘
        └──────────────────┘
                 │
        ┌──────────────────┐
        │     Solve        │
        └──────────────────┘
                 │
        ┌──────────────────┐
        │     strain       │
        │    (output)      │
        └──────────────────┘
```
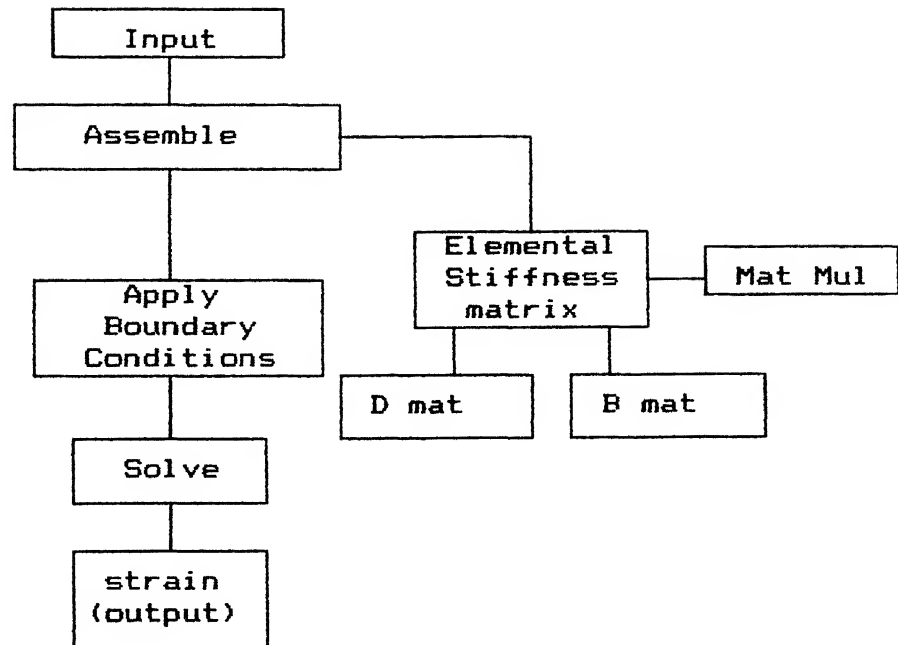
Fig. 2.6 Flow chart for finite element programme

The software has been run on HP 9000 and CONVEX 220 systems. The latter is a minisuper computer approximately six times faster than the super mini HP 9000. The execution time for a mesh of 1384 nodes with 364 elements is nearly 30 seconds on CONVEX.

2.7 TEST PROBLEMS

The programme has been checked using following test problems of which results are known.
1. Large plate with a center crack
2. Large plate with an edge crack

2.7.1. LARGE PLATE WITH A CENTER CRACK

The problem of large plate with center crack under distributed load is solved for stresses and stress intensity factor in Mode I. Figure 2.7. shows the geometry of the specimen and Fig. 2.8, the mesh used.
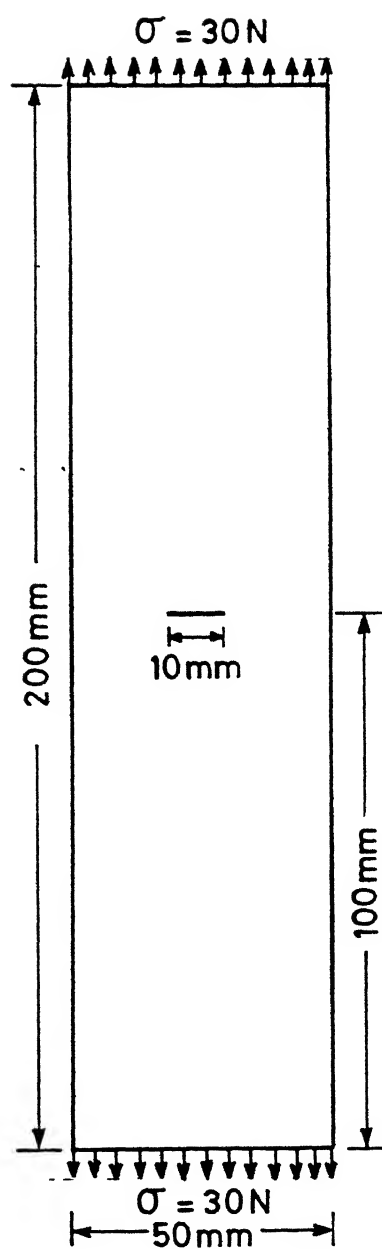
Fig. 2. 7 Problem of Centre Crack
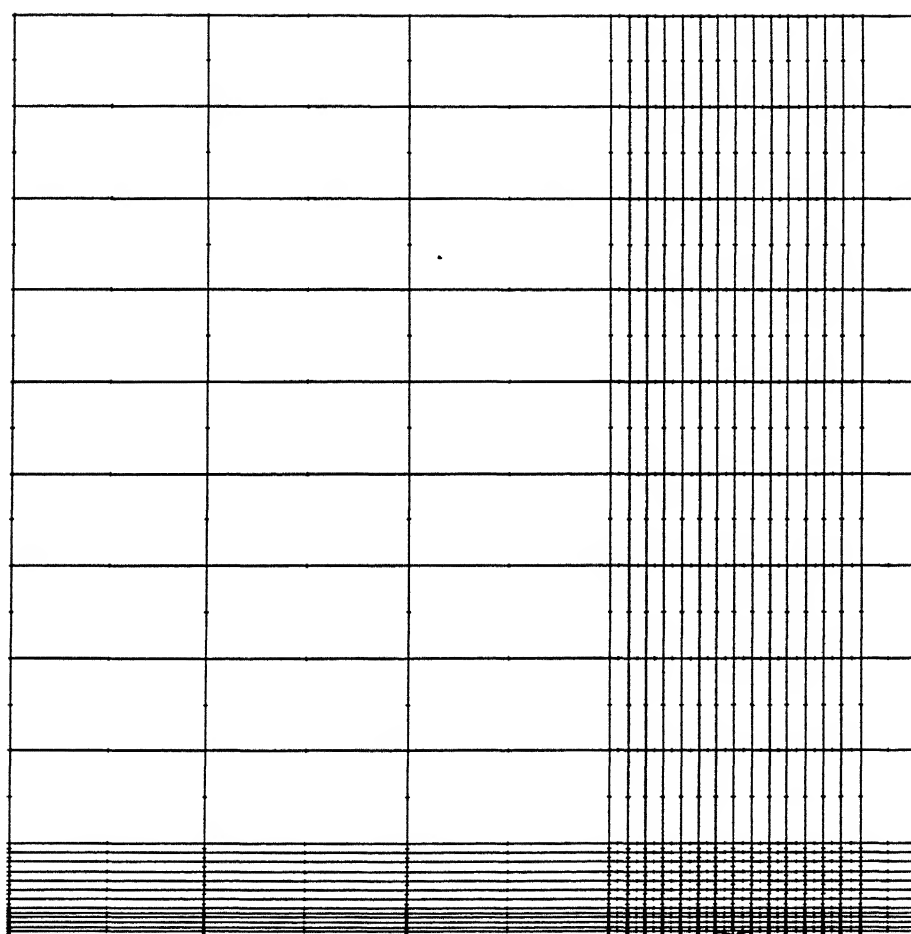
Fig. 2.8 Mesh for Problem of Centre Crack.

The FEM code gave a stress intensity factor of 3.57 MPa$\sqrt{m}$ compared to a value of 3.76 MPa$\sqrt{m}$ from the formula $K=\sqrt{Sec\left(\frac{\pi a}{w}\right)}\sigma\sqrt{\pi a}$ [8]. The two are in close agreement, the numerical result differing from the latter by 5 % only.

Also in this case of large plate, the stress intensity factor gives the stresses near the crack tip through the equations given below [8] :

$$\sigma_x = \frac{K_I}{\sqrt{2\pi r}} \cos\frac{\theta}{2} \left(1- \sin\frac{\theta}{2} \sin\frac{3\theta}{2} \right) - \sigma$$

$$\sigma_y = \frac{K_I}{\sqrt{2\pi r}} \cos\frac{\theta}{2} \left(1+ \sin\frac{\theta}{2} \sin\frac{3\theta}{2} \right)$$

$$\tau_{xy} = \frac{K_I}{\sqrt{2\pi r}} \sin\frac{\theta}{2} \cos\frac{\theta}{2} \cos\frac{3\theta}{2}$$

The stress field obtained numerically and found to be in good agreement with analytical results.

2.7.2. LARGE PLATE WITH AN EDGE CRACK

The geometry of the problem is shown in Fig. 2.9. The stress intensity factor K_I and stresses in opening mode are solved. Figure 2.10. shows the mesh used.

The value of K_I is obtained as 0.32 MPa$\sqrt{m}$ from finite element calculations. This is within 3 % of the value 0.33 MPa$\sqrt{m}$ calculated using the equation $K = 1.12 \sigma\sqrt{\pi a}$. Here also, the stress field is found to be in good agreement with analytical results.

2.8 RESULTS OF DCB SPECIMEN WITH THIN CANTILEVERS

Finally, a DCB specimen of present investigation is analyzed for stresses and SIF. The specimen geometry is the same as in Fig. 2.1. The mesh is shown in Fig. 2.3 and 2.4.
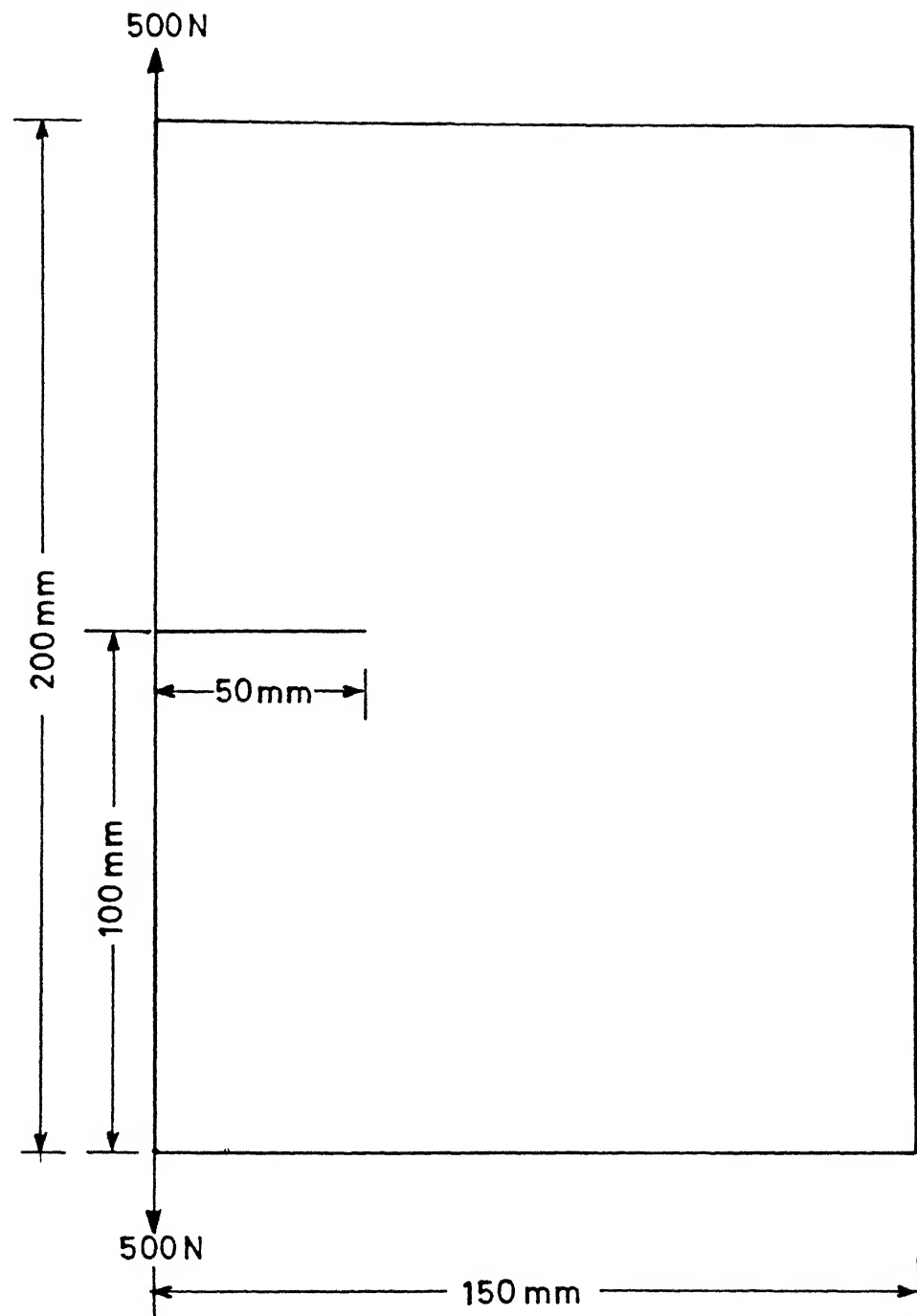
Fig. 2. 9   Problem of Edge Crack
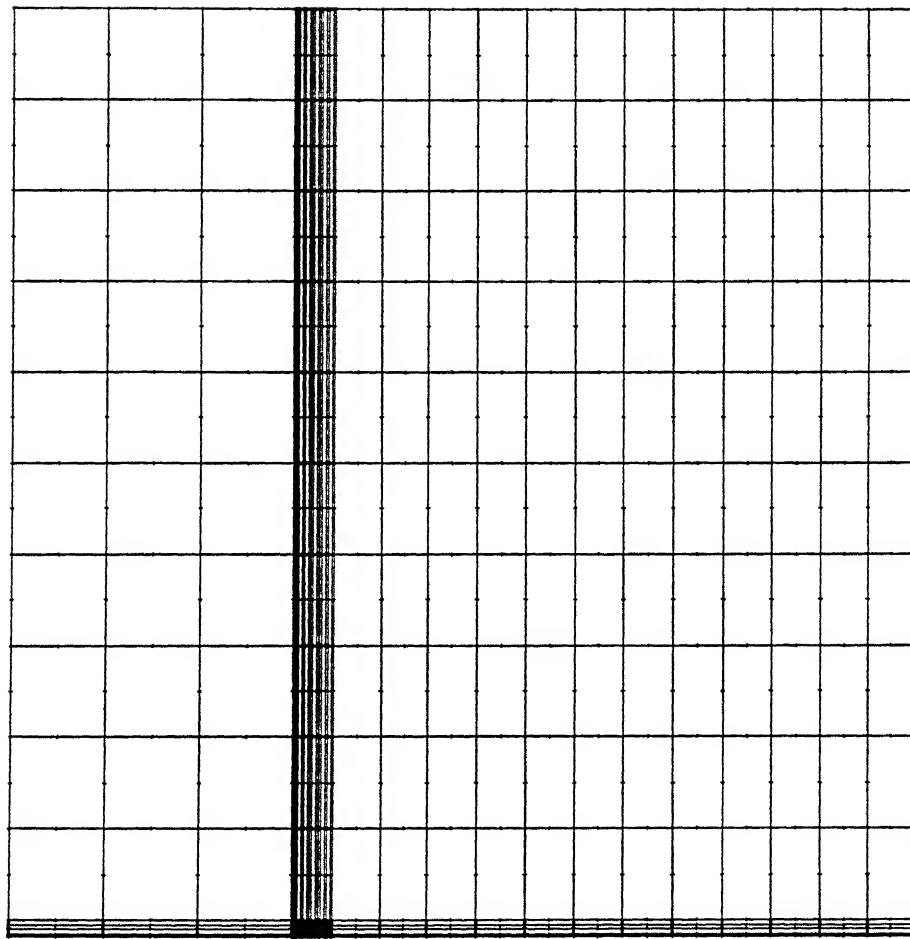
Fig. 2.10 Mesh for Problem of Edge Crack

The value of stress intensity factor is obtained as
1.6 MPa√m̄ from finite element formulation for a load of P = 60N.

2.8.1 Comparison of Numerical Result

For comparison purpose, K_I has also been calculated using
the formula [8]

$$K_I = \frac{2\sqrt{3} \ P \ a}{h^{3/2} \ B(1-\nu^2)} \qquad \ldots (2.18)$$

This method is referred to as ' K_I through G_I approach' in
this study since Eq. 2.18 is derived in an indirect way, first
finding G_I and then using the relation $K = \sqrt{\frac{E \ G}{(1-\nu^2)}}$. The
derivation of Eq. 2.18 is presented in Appendix B.

This analysis provides K_I by knowing load at the cantilever
ends, crack length and specimen dimensions. However, it does
not give any idea of strain field near the crack tip. In fact
obtaining closed form solution for strain field is difficult
task since the free surfaces are very close to the crack tip
and influence the stress/strain field considerably even at
points which are close to crack tip. Because the strain gauge is
of finite dimensions (0.2 mm gauge length and 1.2 mm width),
it cannot be fixed very close (< 1 mm) to the crack tip and
for strain field in a DCB specimen with cantilevers of
thickness less than 3 mm, one is forced to go to the finite
element analysis.

Moreover, it is clear from the derivation that only flexural
energy of the cantilevers has been accounted for and the shear
strain energy caused by the lateral loads and the strain energy
in the bulk material beyond the crack tip have not been
considered in evaluating the compliance, although, the assumption
of neglecting these strain energies is reasonable since the
cantilevers are thin and flexural energy dominates.

Using Eq. 2.18, the value of K_I is obtained as 1.89 MPa√m for load P = 60 N. This differs from the result of finite element analysis by 18 %. The numerical programme has been run for different loads and crack lengths. The results are compared with those calculated through Eq. 2.18 in Table I. The percentage difference between the values obtained through the two methods is consistent.

For comparing the experimental results the numerical value is preferred because it is free from assumptions made in the G_I approach.

TABLE I Comparison between K_I obtained numerically and K_I calculated through equation 2.18

Sl. No.	Load N	Crack length mm	K_I through G_I approach MPa√m	K_I through F.E. analysis MPa√m	diff- erence %
1	58	36.5	2.29	1.89	-18
2	50	36.5	1.98	1.63	-18
3	56	36.5	2.21	1.82	-18
4	70	35.5	2.77	2.29	-17
5	82	30.5	2.71	2.18	-19
6	81	23.5	1.93	1.76	-14

2.8.2 Strain Field and Contours

The results are post processed to obtain the strain field around crack tip in the thin specimen of Fig. 2.1 using a routine developed by Ramesh [12] and strain contours are plotted.

First step while plotting is to solve for the strains at Gauss Points in each element. These strains are then linearly

extrapolated to find strains at the nodes. For extrapolation, the following formula is used [13].

$$
\begin{Bmatrix} \varepsilon_i \\ \varepsilon_{ii} \\ \varepsilon_{iii} \\ \varepsilon_{iv} \end{Bmatrix} = \frac{1}{2}
\begin{bmatrix}
1+\frac{\sqrt{3}}{2\rho} & -0.5 & 1-\frac{\sqrt{3}}{2\rho} & -0.5 \\
-0.5 & 1+\frac{\sqrt{3}}{2\rho} & -0.5 & 1-\frac{\sqrt{3}}{2\rho} \\
1-\frac{\sqrt{3}}{2\rho} & -0.5 & 1+\frac{\sqrt{3}}{2\rho} & -0.5 \\
-0.5 & 1-\frac{\sqrt{3}}{2\rho} & -0.5 & 1+\frac{\sqrt{3}}{2\rho}
\end{bmatrix}
\begin{Bmatrix} \varepsilon_A \\ \varepsilon_B \\ \varepsilon_C \\ \varepsilon_D \end{Bmatrix}
$$

Where ε_A, ε_B, ε_C, ε_D and ε_i, ε_{ii}, ε_{iii}, ε_{iv} each represents one strain component ε_x, ε_y or γ_{xy}. The roman numerical subscripts represent the nodal quantities and the alphabetical subscripts represent the gauss point quantities. In 2 point integration, $\rho = \frac{1}{\sqrt{3}}$ (Fig. 2.11). The principal strains and their orientations are then determined at each node. For finding the principal strains, the following formula is used [14]

$$
\varepsilon_{1,2} = \frac{\varepsilon_x + \varepsilon_y}{2} \pm \sqrt{\left(\frac{\varepsilon_x - \varepsilon_y}{2}\right)^2 + \left(\frac{\gamma_{xy}}{2}\right)^2}
$$

The orientations of the principal strains are calculated by solving for eigen vectors of the strain matrix corresponding to ε_1 and ε_2 which are eigen values.

2.8.3 Results

The strain fields are given in Fig. 2.12 to 2.14. All the plots are for the upper cantilever. Fig. 2.12 gives the strains along the y-axis and Figure 2.13 shows the strains along x-axis. It is clear that the strain values are high near the crack tip. The principal strains are also plotted which is shown in Fig. 2.14.
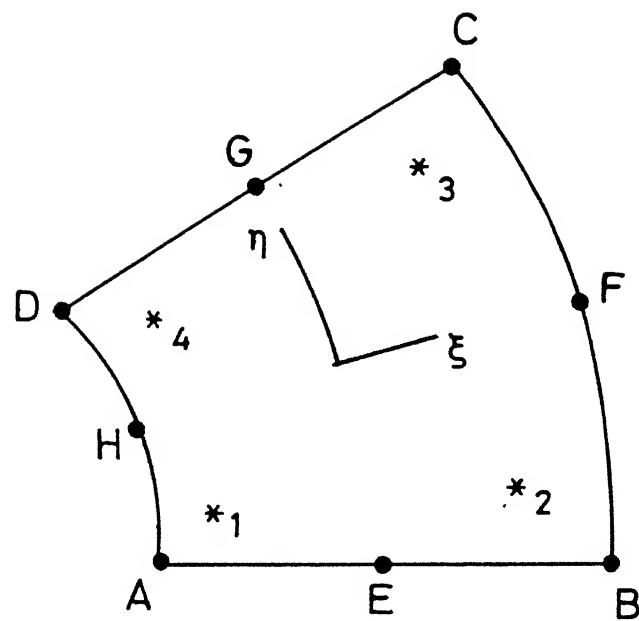
Fig. 2.11 Element to Explain Extrapolation
of Stesses

2.8.4 Location of Strain Gauge

It is noted that the points which lie on the line of intersection of the neutral plane of the upper cantilever and the side face of the specimen and close to the crack tip has relatively high strains suitable for measurement and does not _ ·;~rience any bending strain after the crack tip passes the point. Of these points, the one which is at a distance of approximately 1.5 mm from the crack tip (measured parallel to the x-axis) experience maximum strain

At this point, the orientation of principal strain is approximately 48° with the x- axis (Fig. 2.15) and hence it is decided to fix the strain gauge at a convenient angle of 45°. Figure 2.16 shows the strain contours along 45° direction. The location of strain gauge and the area covered by it are shown in Fig. 2.17.

TOTAL NO. OF NODES =   1635   TOTAL NO. OF ELEMENTS = 512

zero value

zero value

1

		WINDOW NO.	WINDOW SIZE				C.L.D.
—————	+ve value						
– – – – –	−ve value	1	27.00	33.00	2.80	5 60	.00002
—————	zero value	2	.00	.00	.00	.00	.00000
C.L.D–CONTOUR LEVEL DIFF.		3	.00	.00	OO	OO	.00000

Fig. 2.12 $\mathcal{E}_{yy}$ for DCB Specimen with Thin Cantilevers

OTAL NO. OF NODES =   1635   TOTAL NO OF ELEMENTS = 512

		WINDOW NO.	WINDOW SIZE			C.L.D.
_____	+ve value					
- - - - - - - -	-ve value	1	27.00	33.00	2.80 5.60	.00002
_____	zero value	2	.00	.00	.00 .00	00000
C.L.D-CONTOUR LEVEL DIFF.		3	.00	.00	.00 .00	.00000

Fig. 2.13 ε_{xx} for DCB Specimen with Thin Cantilevers

TOTAL NO OF NODES =   1635   TOTAL NO. OF ELEMENTS = 512

zero value

		WINDOW NO.	WINDOW SIZE			C.L D.
———————	+ve value					
– – – – – – – – –	-ve value	1	27.00	33.00	3.00	5.60	.00002
———————	zero value	2	.00	.00	.00	.00	.00000
C.L.D-CONTOUR LEVEL DIFF.		3	.00	.00	.00	.00	00000

Fig. 2.14 Principal Strains for DCB Specimen with
         Thin Cantilevers

TOTAL NO. OF NODES = 1635   TOTAL NO. OF ELEMENTS = 512

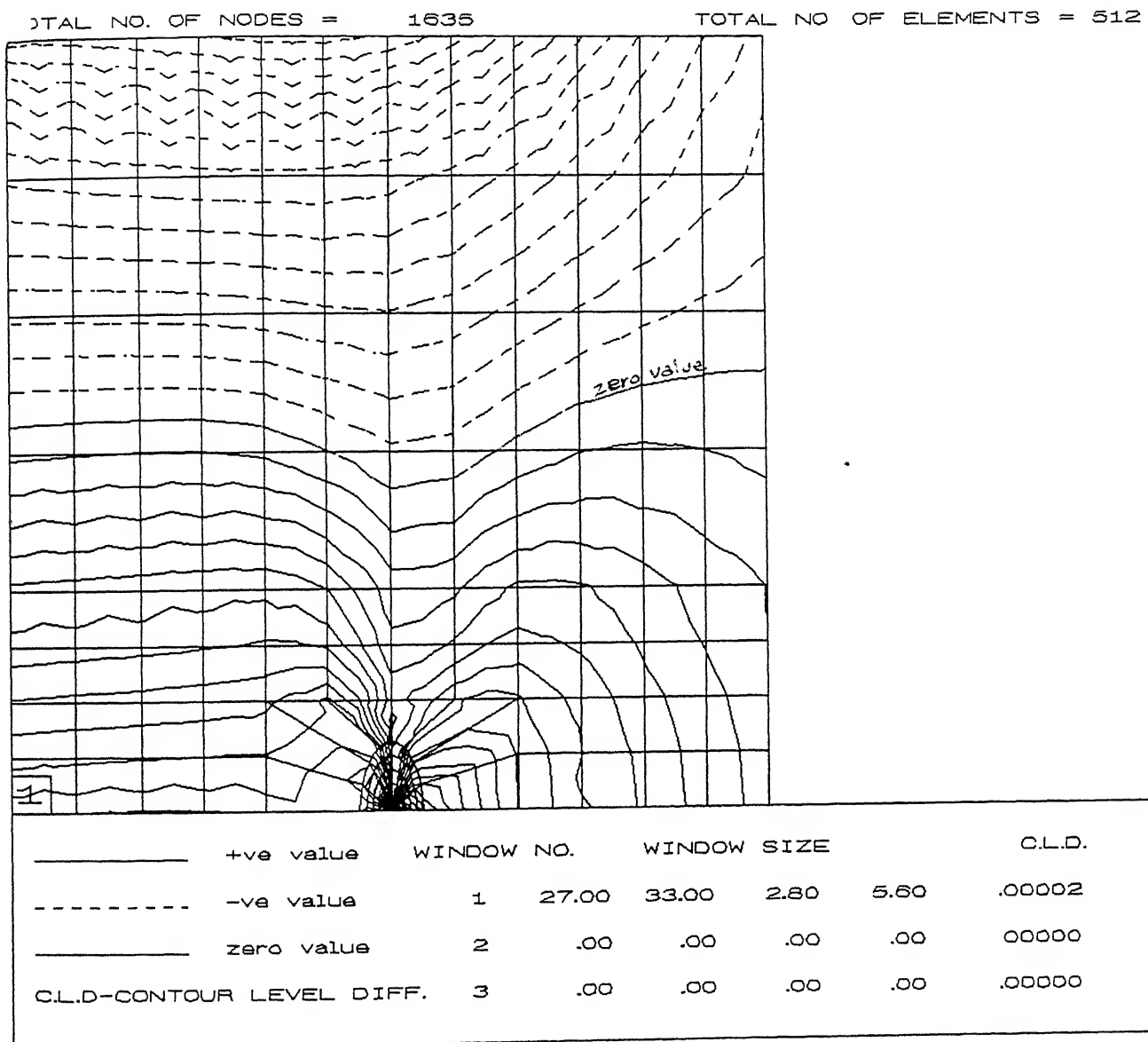|		WINDOW NO.	WINDOW	SIZE		C.L.D.
———————	+ve value					
- - - - - - - -	-ve value	1	27.00	33.00	3.00	5.60	15.00000
———————	zero value	2	.00	.00	.00	.00	.00000
C.L.D-CONTOUR LEVEL DIFF.		3	.00	.00	.00	.00	.00000
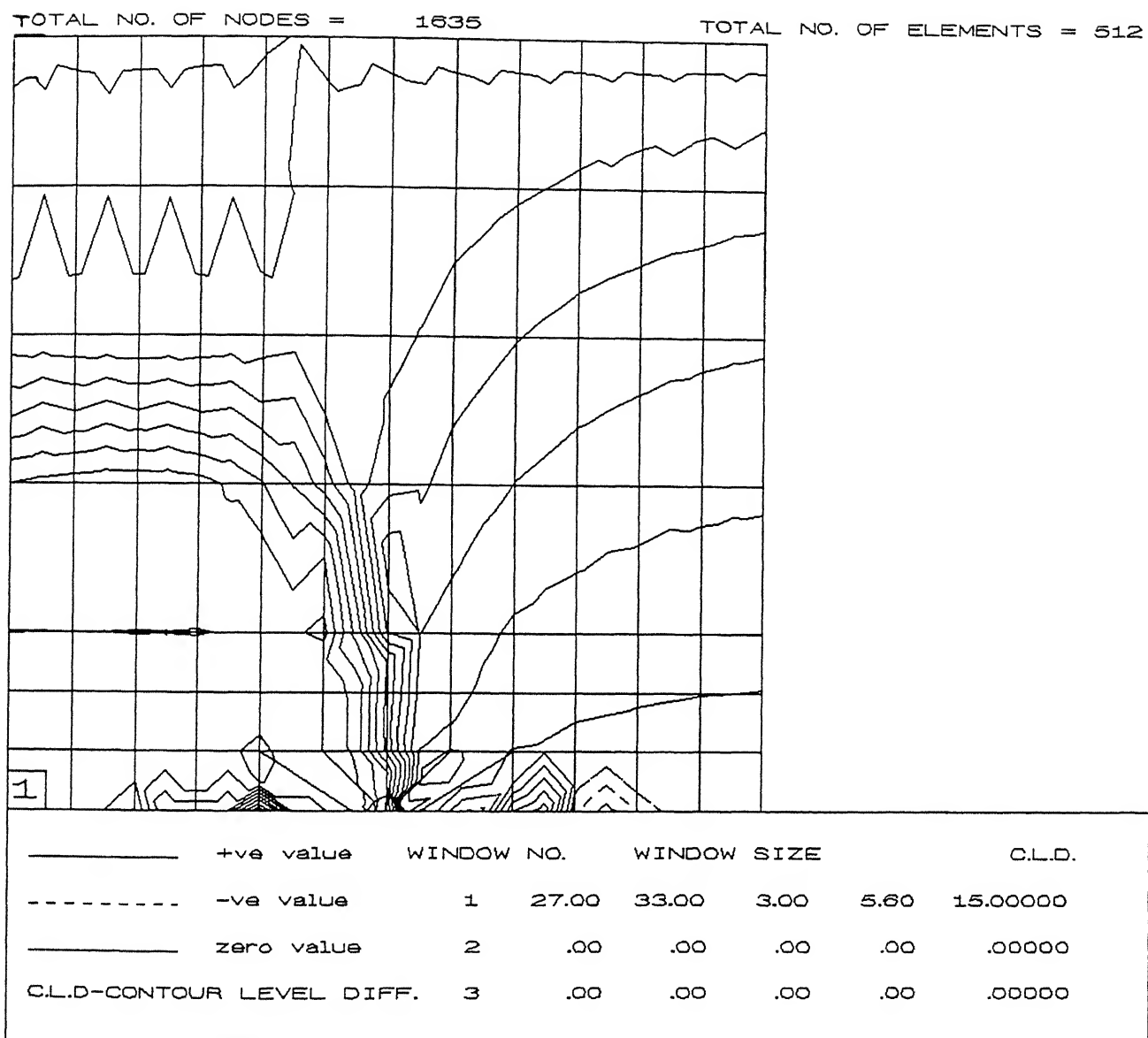
Fig. 2.15 Orientations of Principal Strains for DCB Specimen
          with Thin Cantilevers

TOTAL NO. OF NODES =   1635   TOTAL NO. OF ELEMENTS = 512

zero value

		WINDOW NO.	WINDOW SIZE			C.L.D.
————————	+ve value					
— — — — — — —	-ve value	1	30.00 35.00	3.00	5.60	.00002
———·————	zero value	2	.00 .00	.00	.00	.00000
C.L.D-CONTOUR LEVEL DIFF.		3	.00 .00	.00	.00	.00000
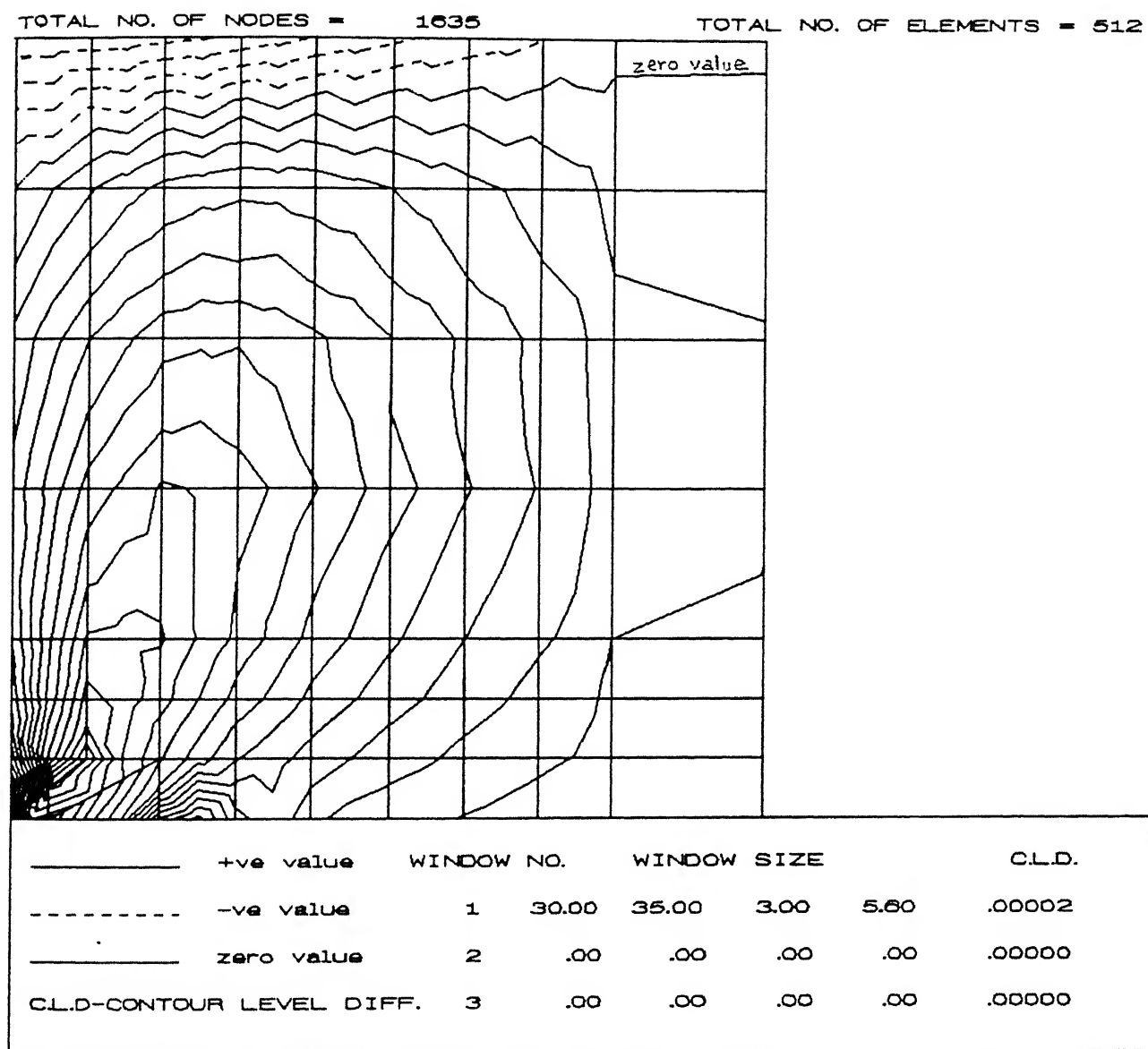
Fig. 2.16   Strains along Direction that is at 45°
with X-aixs.

0.5 mm

TOTAL NO. OF NODES = 1635   TOTAL NO. OF ELEMENTS = 512

STRAIN GAUGE

zero value

45°

0.5 mm

CRACK

0.2 mm

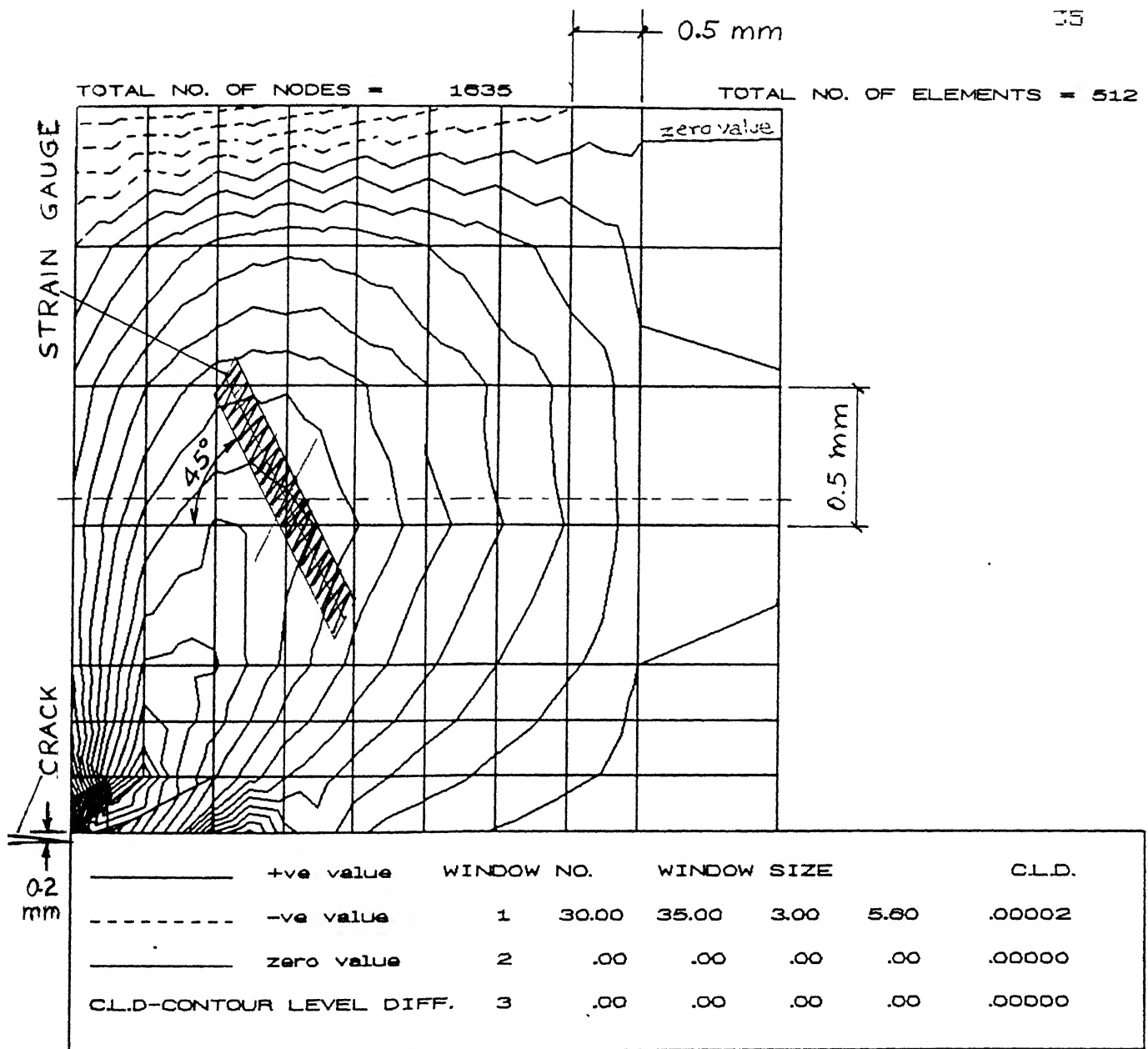|		WINDOW NO.	WINDOW SIZE				C.L.D.
————	+ve value						
- - - - - -	-ve value	1	30.00	35.00	3.00	5.60	.00002
—— · ——	zero value	2	.00	.00	.00	.00	.00000
C.L.D-CONTOUR LEVEL DIFF.		3	.00	.00	.00	.00	.00000

Fig. 2.17 Strains along 45° with Strain Gauge Location.

CHAPTER III

EXPERIMENTAL TECHNIQUE

3.1 INTRODUCTION

This chapter deals with experimental details including design and preparation of specimen, equipment used, parameters controlled and measurements made during the experiment. The experiment is conducted under controlled displacement condition so as to obtain a quasi-static crack growth.

3.2 SPECIMEN GEOMETRY AND MATERIAL

GEOMETRY

The DCB specimen used has two thin metal strips joined together with epoxy. The crack length is varied between 23.5 and 36.5 mm and the thickness of the cantilevers is 2.78 mm each. Figure 2.1 provides information on the geometry.

MATERIAL

The material used is hardened alloy steel, 40Ni2Cr1Mo28[*] (EN24), which has a high yield stress value after hardening. Hardening is done by keeping the metal at 830 - 850 ^{o}C for one hour and then quenching in oil. This is followed by annealing to relieve the residual stresses. In annealing, the metal is heated to about 310°C for a period of nearly 20 minutes accompanied by furnace cooling. The hardness of the strips is then checked. In the present case the average hardness of the strips on C-scale is 33 which corresponds a yield stress of nearly 1000 MPa. Each strip was ground flat and polished with alumina powder.

BONDING

The faces of the metal strips to be bonded using epoxy are etched to give better inter facial strength. The etching was done by dilute Nitric Acid. For bonding, epoxy LY 556 and hardener HY 1907IN in the ratio 100:85 by weight are used. To this mixture, accelerator DY 062 also is added at the rate of 1.5 ml per 100 gm of epoxy. The resin, the hardener and the accelerator are supplied by Ciba-Geigy Limited, Bombay. The sides of the specimen are covered with a layer of wax to prevent them from getting coated with epoxy and the faces to be bonded are cleaned with pure acetone. The mixture is then applied to the cleaned faces. The two strips are then put together and pressed in specially built fixture made of two stiff steel plates (each 25mm thick) with ground flat faces (Fig. 3.1). Between the strips and the flats of the fixture, a sheet of BOPP was placed on each side that works as a release film.

Provisions are made in the fixtures for keeping the two strips in position while curing. The base plate of the fixture has two cylindrical stops and three adjustable buttons. Both the thin strips are butted against the cylindrical stops and kept in place with the adjustable buttons. Each adjustable button has slot of 4 X 7 mm so that they can be tightened to the base at a desired location. Also, these buttons have different heights so as to hold each strip in its place.

The fixture along with the specimen is placed between two platens of a hydraulic press. The platens are heated through inbuilt heaters and the temperature of the specimen is monitored by placing a chromel-alumel thermocouple. The temperature of the specimen is maintained at 130° C under 1.2 MPa pressure for one hour. It is then allowed to cool under the same pressure to room temperature.

PRECRACK

While bonding the strips, a crack is introduced by placing a film of Biaxially Oriented Poly-Propylene (BOPP) up to the required length so that the strips are not bonded there. For experiments of this study, crack length is varied between 23.5 and 36.5 mm.

3.3 HINGES

Hinges have been designed and fabricated for applying load to the cantilever ends (Fig. 3.3). For fixing the hinges, two tapped holes have been provided at the ends of the cantilevers as shown in Fig. 2.1.

Each hinge consists of a bracket, a support and a pin all made of steel. The bracket is fixed to the cantilever with the help of two high strength capscrews. The support is inserted into the bracket and the pin is used to join the two. The 10 mm diameter pin makes the hinge strong and stiff. All the holes of the hinges and the diameter of the pin are made with close tolerances. The end of the support is cylindrical of diameter 12mm, made to fit the inside loading fixture of the tension machine, INSTRON 1195.

The hinge so designed is moment free while load is applied. Further, it keeps the load line always vertical.

3.4 EXPERIMENTAL DETERMINATION OF G_{IC}

A preliminary experimental study was conducted to have some idea about the maximum load as well as order of G through the standard technique of successive growth of the crack. The details of the technique are given in [15]. Knowing G_{IC}, one can evaluate K_{IC} by using the well known relation $K_{IC} = \sqrt{G_{IC}E/(1-\nu^2)}$.

3.5 EXPERIMENTAL DETERMINATION OF K_{IC}

3.5.1 Introduction

This constitutes the major objective in the present work. The idea here is to correlate strain measurements in the vicinity of the crack tip through a strain gauge with stress intensity factor for a DCB specimen with thin cantilevers. The loads are applied in displacement control mode with a very slow cross head speed. This work is expected to pave way for a more widespread use of strain gauges in this field. It is hoped that this procedure could be extended to dynamic problems also.

3.5.2 Strain Gauges

The strain gauges used in these experiments have been supplied by Tokyo Sokki Kenkyujo Co.,Ltd., Japan. They have a gauge length of 0.2 mm and a gauge width of 1.5 mm. The base of the strain gauge is rectangular with dimensions 3.5 mm X 2.5 mm. Its resistance is 120 +0.3 Ω and gauge factor, 2.07. Figure 3.4 shows the details of the strain gauge.

Fixing of Strain Gauges

Extreme care is taken in fixing the strain gauges as it has only a very small area for bonding. Epoxy LY 556 and hardener HY 951 are used in bonding. The two are mixed well in the ratio 10:1 by weight. The ambient temperature is kept around 55 to 60°C for about 24 hours to help curing. Localized pressure is applied while the curing takes place.

Positioning of the strain gauge is done with the help of a fixture made out of self sticking paper. It gives a corner and two sides as reference for fixing the strain gauge (Fig. 3.5). The efficiency of this method is checked from the observations made under travelling microscope which showed the center of the strain gauge to be very near to the point required, the error being less than 0.1mm.
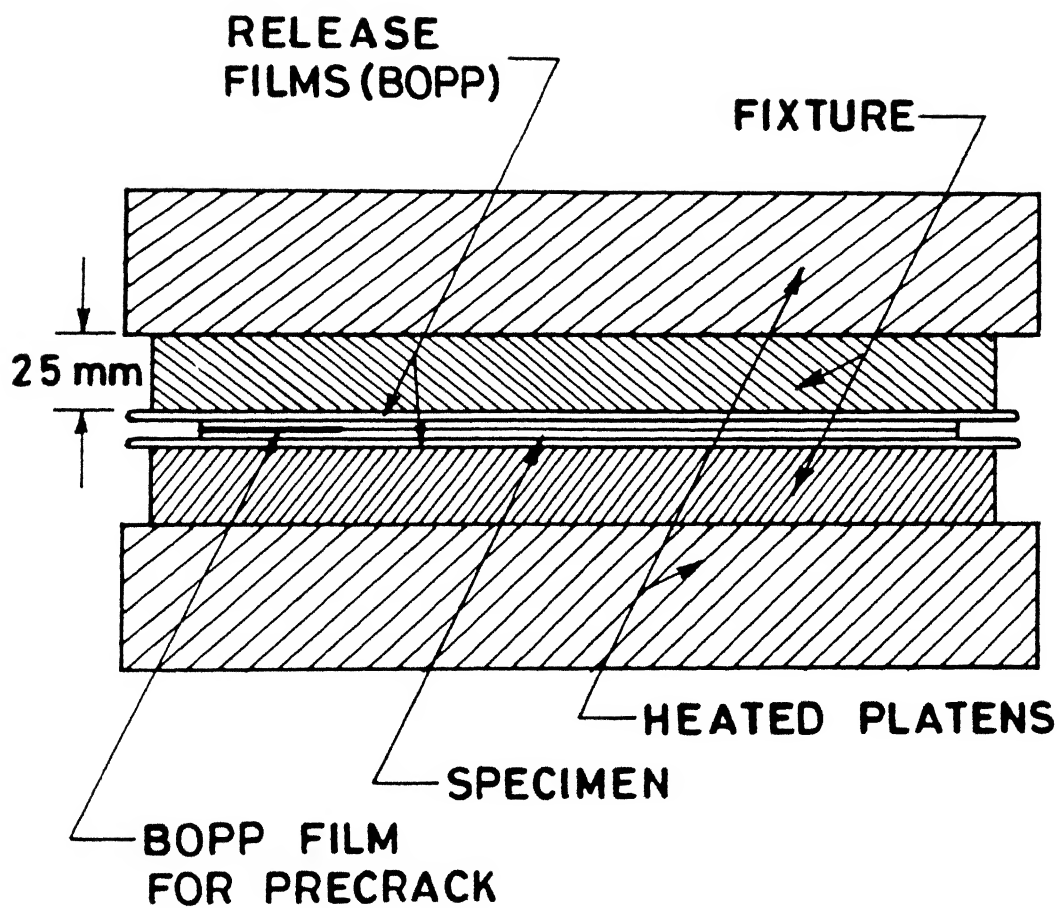
RELEASE
FILMS (BOPP)

FIXTURE

25 mm

HEATED PLATENS

SPECIMEN

BOPP FILM
FOR PRECRACK

Fig. 3.1 Pressing of Two Steel Cantilevers for Bonding them with
Epoxy at High Temperature and Pressure with a pre-crack

3.5.3 Measurement of Strain

The strain gauge output is measured using strain indicator (Model P-350A, Measurement Group). The crack velocity being very small the strain indicator can be conveniently used. The strain indicator has a least count of 1 μ and hence provides reasonably accurate observations. The measurement is made continually at regular intervals of time.

3.5.4 Equipment

The experiment is conducted on INSTRON, model 1195. This is a highly flexible machine and can be used for testing materials in tension, compression, flexure and torsion. This has two main units namely an electronic control console and a loading frame. There is a chart recorder system also which is used in our experiments to plot the displacement against load. INSTRON has a maximum load capacity of 100 kN and a lowest cross head speed of 0.05 mm per minute. The cross head speed can be maintained constant with an accuracy of $\pm$ 0.1 % when averaged over 20 mm of travel at constant load.

3.5.5 Procedure

The specimen is mounted on the INSTRON machine and the trailing end of the specimen is suspended by ~ ... end to keep the axis of the specimen horizontal. It is a pulley like arrangement so that the specimen as a whole can move up and down but remains always horizontal.

The specimen is loaded in displacement controlled mode and the cross head speed is fixed at 0.1 mm/minute. From the preliminary experiments it was observed that the crack velocity remains quite low under such a displacement rate. Since the maximum load during the initial experiments was in the range of 50 - 75 N, the full scale load on the machine is kept 100 N. The chart speed for recording the graph displacement versus load is maintained at a convenient value of 10 mm/minute. In this machine, the upper jaw is fixed and the lower jaw moves down thus applying the load.

Once the experiment is started and the load reaches around half the expected maximum load, recording of the strain indicator readings is started. Once the crack has moved well past the strain gauge, the specimen is unloaded and the readings are noted while unloading also. The entire experiment lasts for approximately 20 minutes.

3.5.6 Data analysis

The experiments were conducted with the strain gauge fixed at a suitable distance from the center line of the hinges so that it is at about 5 to 8 mm from the tip of the precrack. The smaller value is used in the case of smaller crack lengths. From the numerical analysis, it is estimated that the maximum value of strain recorded will be when the crack tip is 1.5 mm away from the strain gauge. Hence, the crack length corresponding to the peak obtained in the strain plots can be deduced. We find that for a crack length of 30 mm and load of the order of 60 N, the maximum strain expected is around 140 microns according to numerical prediction. The graphs and other results of the experiments are shown in subsequent pages.

3.6 CHECKING OF STRAIN GAUGE

The performance of the strain gauge of 0.2 mm gauge length has been checked by measuring the bending strain in a cantilever in static condition. The error in measurement was found to be within 5 %.
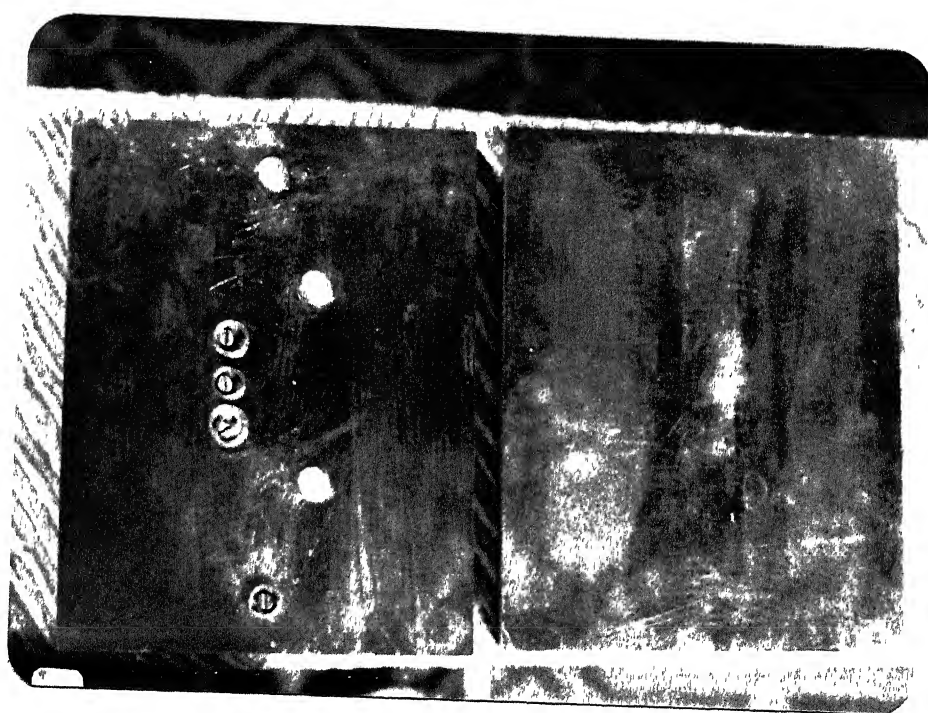
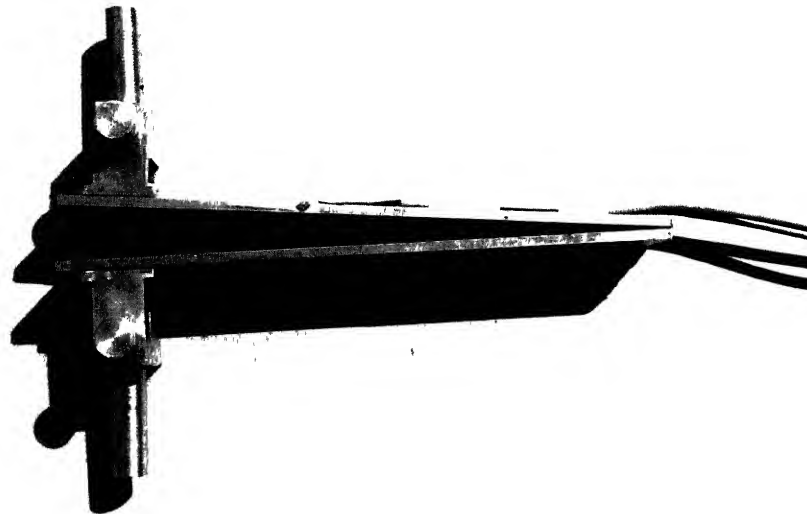Fig. 3.2   Photograph of Base Fixture used in Curing

Fig. 3.3(a) Overall View of the Specimen with
Hinges and Strain Gauge

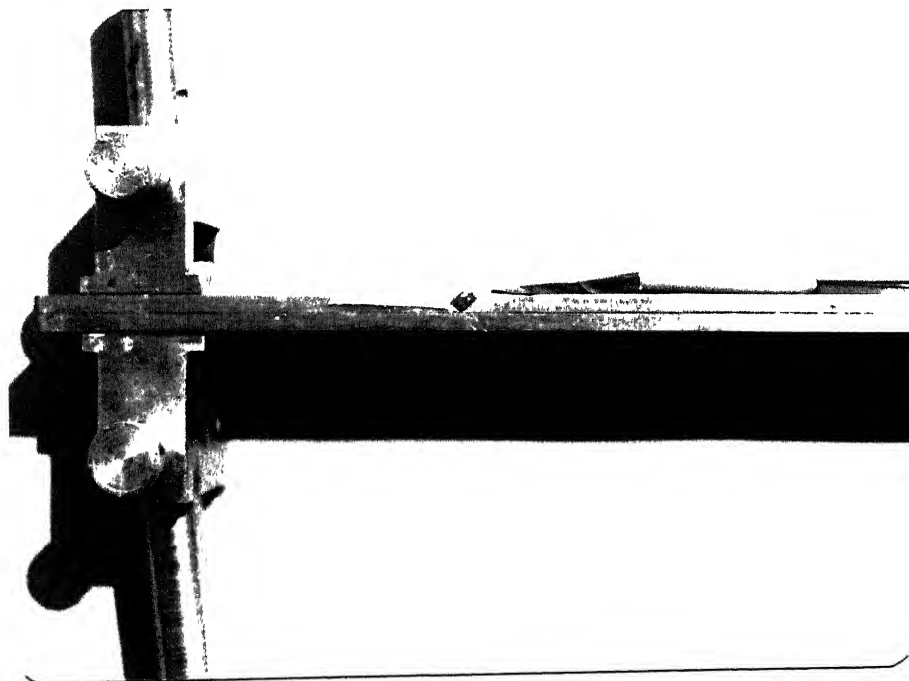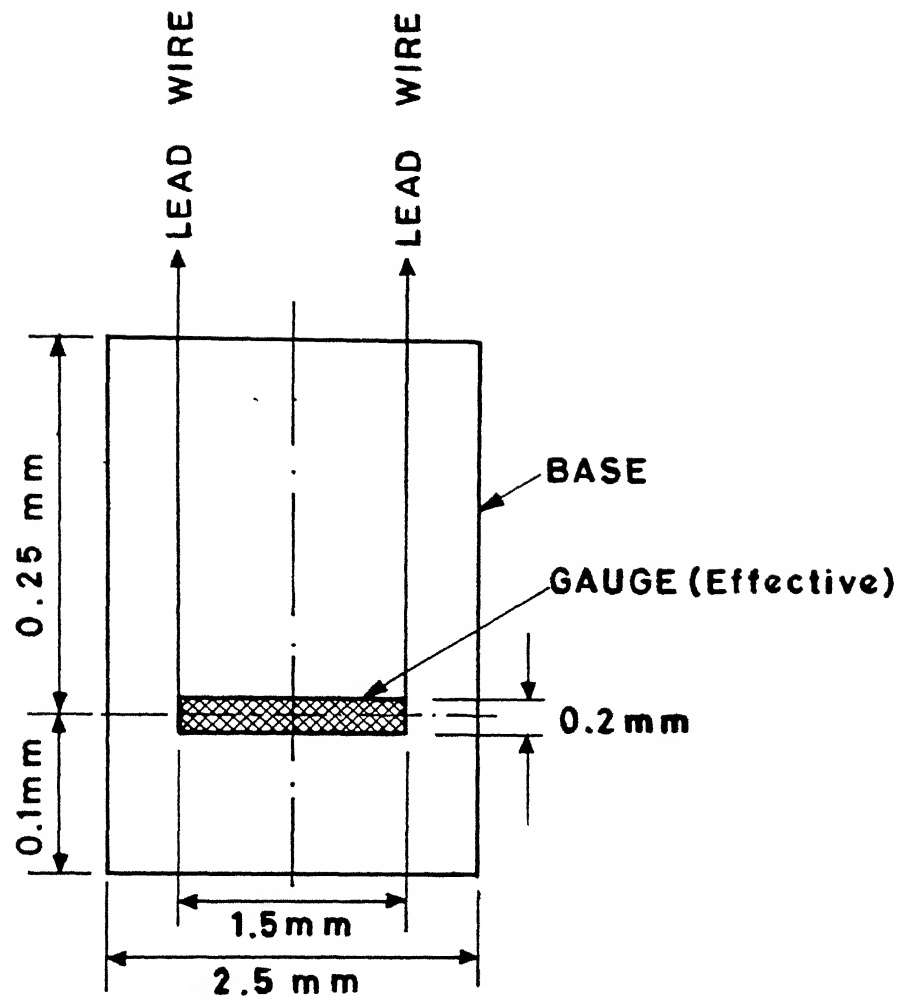Fig. 3.4(b) Near View of Strain Gauge and Hinges
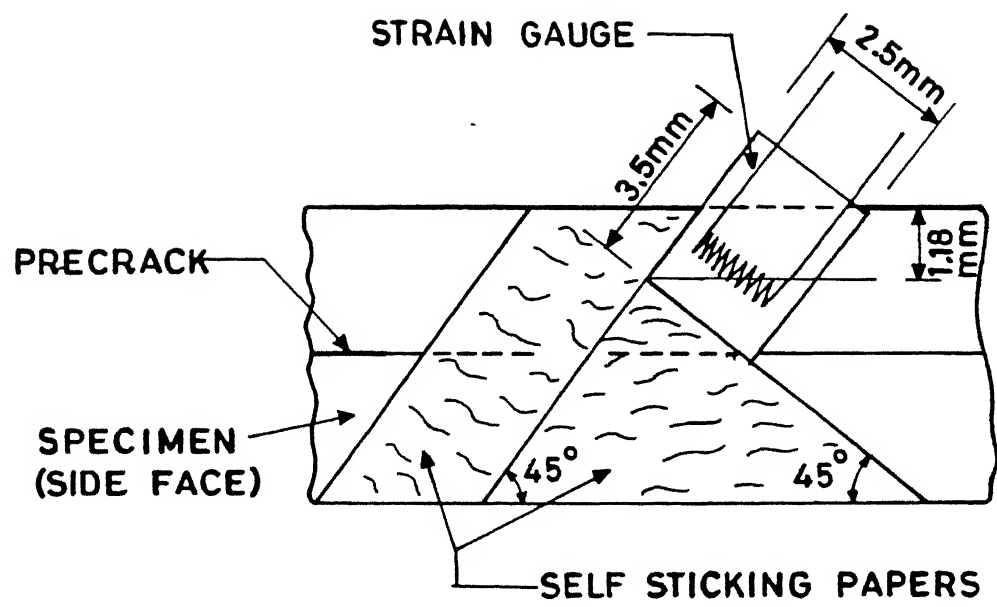
Fig. 3.4   Detailed Figure of Strain Gauge.

STRAIN GAUGE

2.5mm

3.5mm

PRECRACK

1.18 mm

SPECIMEN
(SIDE FACE)

45°

45°

SELF STICKING PAPERS

Fig. 3.5 Fixture for Strain Gauge through Self Sticking Papers.

CHAPTER IV

RESULTS AND DISCUSSIONS

4.1 INTRODUCTION

The strain field in the DCB specimen with thin cantilevers has been obtained through finite element technique and used in selecting proper location for fixing a strain gauge for strain measurement as described in section 2.8.3. After gluing the strain gauge of 0.2 mm gauge length in the proper position (Fig. 2.18), the specimen is loaded in a tension machine in Mode I at a very low crosshead speed. The load applied at the ends of the cantilevers is recorded through a strip chart recorder of the tensile machine.

As the load is increased, a stage is reached when the crack starts propagating. The rate of propagation is very slow and the strain output of the gauge is recorded with a strain indicator at regular intervals of time. Starting from zero when the load is zero, the strain increases as the crack comes near the strain gauge, reaching a peak. The strain then starts decreasing as the crack passes the strain gauge. Knowing the peak strain, the crack length, K_{IC} is calculated making use of the numerical programme.

For comparison purposes, K_{IC} is determined by two other methods from the load recorded in the strip chart recorder corresponding to the peak strain. In the first method, K_{IC} comes out as a closed form solution described in section 2.8.1 and in Appendix B and is called 'K_I through G_I approach' in this study. The second method finds K_{IC} directly through the finite element scheme developed in chapter II.

Here it may be noted that the value obtained by finite element analysis is preferred to the one obtained through G_I approach as explained in Sec. 2.8.1.

4.2 NUMERICAL SIMULATION

The finite element programme developed in chapter II to determine strain field in a DCB specimen with thin cantilevers has been used for two purposes, (i) to develop a relation between K_I and measured strain for a chosen crack length and (ii) to determine K_{IC} in terms of load at cantilevers' ends.

4.2.1 Relation between K_I and Measured Strain

A relationship is developed between the strain at a point where strain gauge is bonded and the corresponding K_{IC}. The relationship is independent of the cantilever loads.

It should be noted that the specimen is made of hardened alloy steel with very high yield stress. Consequently, the plastic zone at the crack tip is negligibly small especially for this study where loads and strain fields are small. The strain field can be considered to be elastic. Then for a given geometry and crack length strain ε_{ij} at any point of the specimen is proportional to the applied load, P.

$$\varepsilon_{ij} \alpha P \qquad \ldots (4.2)$$

$$\text{and} \quad K \quad \alpha P \qquad \ldots (4.3)$$

By eliminating P, one obtains

$$K \alpha \varepsilon_{ij} \qquad \ldots (4.4)$$

Thus any value of P can be chosen for running the computer programme. However, P should not be very large as it would introduce geometric nonlinearity.

For example with crack length a= 36.5 mm for the specimen size given in chapter III, the programme was run for arbitrarily chosen cantilever load P = 60 N. The peak strain ε_p along the length of strain gauge is found to be related to K_I by the expression

$$K_I = 0.00112 \, \varepsilon_p \qquad \qquad \ldots (4.5)$$

Here K is expressed in MPa√m and ε_p is in microns. This relationship is used to process data. However, the relationship depends on crack length and whenever crack length is changed the programme has to be run to establish the relationship.

4.2.2 Numerical Determination of K_{IC}

The linear relationship between the load applied at the end of the cantilevers and K_I is obtained from the numerical programme for a given crack length. Corresponding to the position of the peak strain, the crack length is known (Sec. 2.8.4).

Considering the same example as in Sec. 4.2.1, the relationship is obtained as

$$K_{IC} = 0.0395 \, P \qquad \qquad \ldots (4.6)$$

Here also, the relationship is worked out by running the finite element code whenever crack length is changed.

4.3 EXPERIMENTAL RESULTS

A total of six experiments were conducted in this study. The crack length for each experiment is shown in column I of Table II. In each experiment, Load vs. Crack Opening Displacement (COD) and Strain vs. COD are recorded. The COD is directly recorded by the strip chart recorder. The chart speed and crosshead speed have been maintained at 10 mm/minute and

0.1mm/minute respectively. Hence 10 mm movement of the chart corresponds to a COD of 0.1 mm. The chart recorder plots the COD against the load applied. The strains measured through a strain indicator are then plotted on the same graph.

For explaining the results of the experiment, the observations of the first experiment are considered. Figure 4.1 shows two curves for experimental results. It is found that the observed peak strain is 138 μ. Using this value of ε and Eq.4.4, the value of K_{IC} is obtained as 1.55 MPa√m. This is referred to as experimental K_{IC} in column IV of Table II.

The load corresponding to the peak strain can also be read from the same figure as 58 N. Also, in this particular experiment, the strain gauge was at a distance of 38 mm from the hinges(load points). As mentioned in Sec. 2.8.4, the crack length corresponding to the peak is 36.5 mm. Now, for these values, the K_{IC} value is predicted as 2.29 Mpa√m through G_I approach using Eq. 2.18.

Similarly invoking linearity, K_{IC} can also be calculated as 1.89 MPa√m using Eq. 4.6. The numerical value is less than the result obtained through Eq. 4.1 by 18 %.

The difference in the numerical and experimental values is 18 %. It is also seen that the value obtained from the experiment is smaller.

Figures 4.2 through 4.6 give the graphs for the other five experiments conducted. In each experiment, measured strain increases as the crack tip approaches the strain gauge, reaching a sharp and distinct peak. In these experiments also, the stress intensity factors are calculated as explained above. The corresponding analytical and numerical values of K_{IC} also are calculated. The results are tabulated in Table II. The last column shows the percentage difference between experimental and numerical K_{IC} values.

Table II shows that results of numerical simulation and G_I approach match well. In all the six cases, G_I approach predicts K_{IC} higher but within 18 %. This difference is expected as explained in Sec. 2.8.1 and so this validates the finite element programme. However the results of numerical simulation is regarded to be more accurate as explained in Sec. 2.8.1. Therefore the experimentally recorded K_{IC} is compared with K_{IC} obtained through numerical simulation in Col. VII of Table II.

Measured strain is consistently lower. Accuracy of small strain gauges of 0.2 mm gauge length has been checked separately through a static test (Sec 3.6) and the error was found to be within 5 %. Imperfect bonding with entrapped air bubbles is thought to be the reason for the discrepancy since such a situation will lead to change in strain field leading to incorrect analysis.

It is expected that the strain gauge reading would be zero after the crack has passed the gauge since the location of the strain gauge is such that the bending strains are zero. Instead it is seen that the strain reading assumes another level and remains there even after unloading. The difference varies considerably from one experiment to another. One of the specimen was checked after the two cantilevers were bonded under high pressure and temperature but before it was loaded. A slight curvature was observed which developed during the curing. As the strain gauge was glued to the prestressed DCB assembly, it did not show any strain until the crack passes through the strain gauge and prestressing is relieved.

In order to keep the prestressing to low values, a new fixture was made after the first four experiments. The improved fixture provides ground flat and very stiff surfaces above and below the specimen while curing. Experiments 5 and 6 were conducted on specimens prepared this way. Of these two

experiments, the effect is evident in the latter where the drop
is only 10 microns compared to a peak of 120 microns.

To sum up, a small strain gauge of 0.2 mm gauge length
bonded at 45° to the crack plane is able to measure strain at
about 2 mm radial distance from the crack tip. A distinct peak
in measured strain is recorded as the crack passes under the
strain gauge. Knowing the peak strain, K_{IC} is determined using
the computer programme. For comparison, the load at the ends of
the cantilever recorded at the instant of peak strain provides
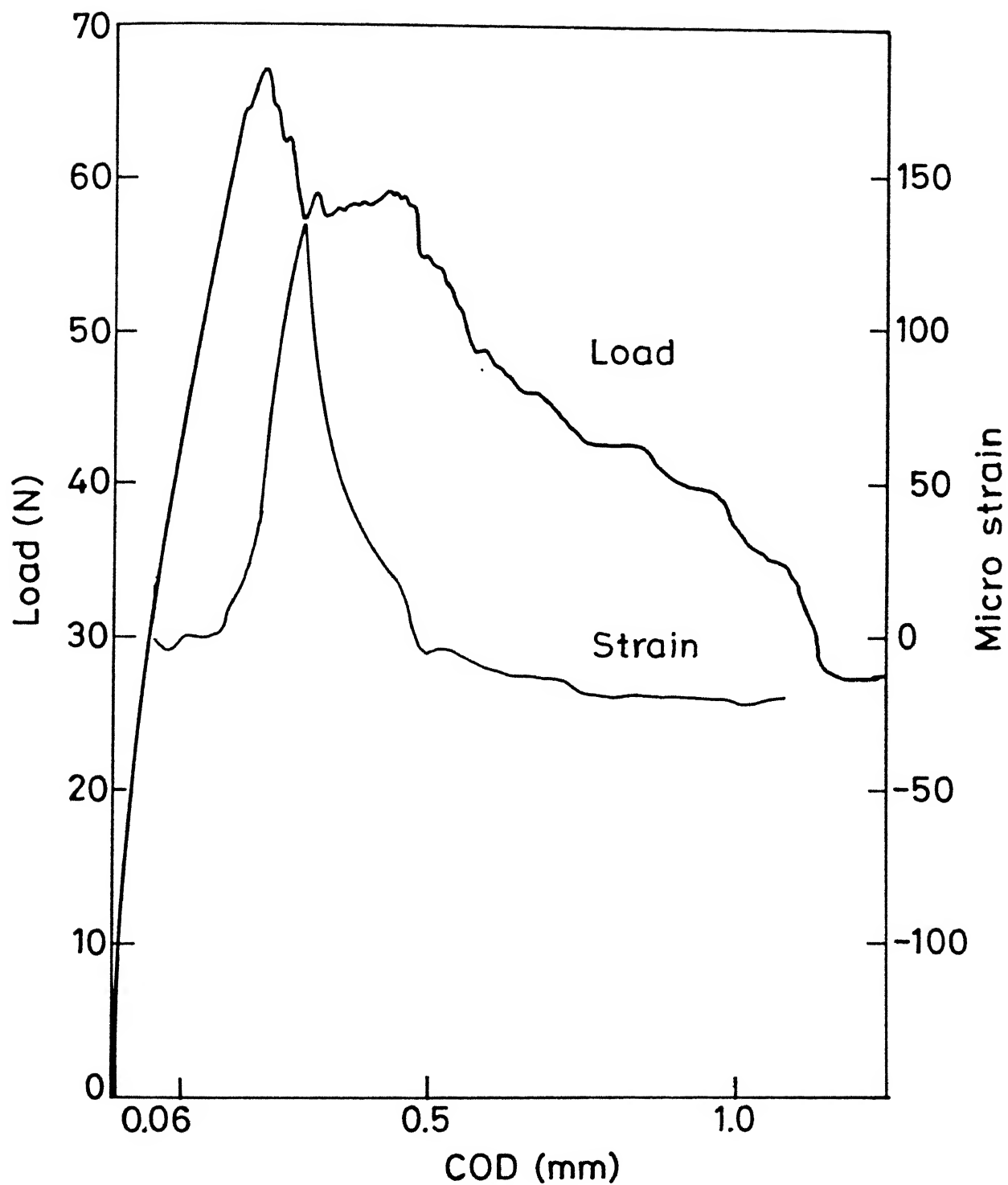the K_{IC} through numerical simulation.

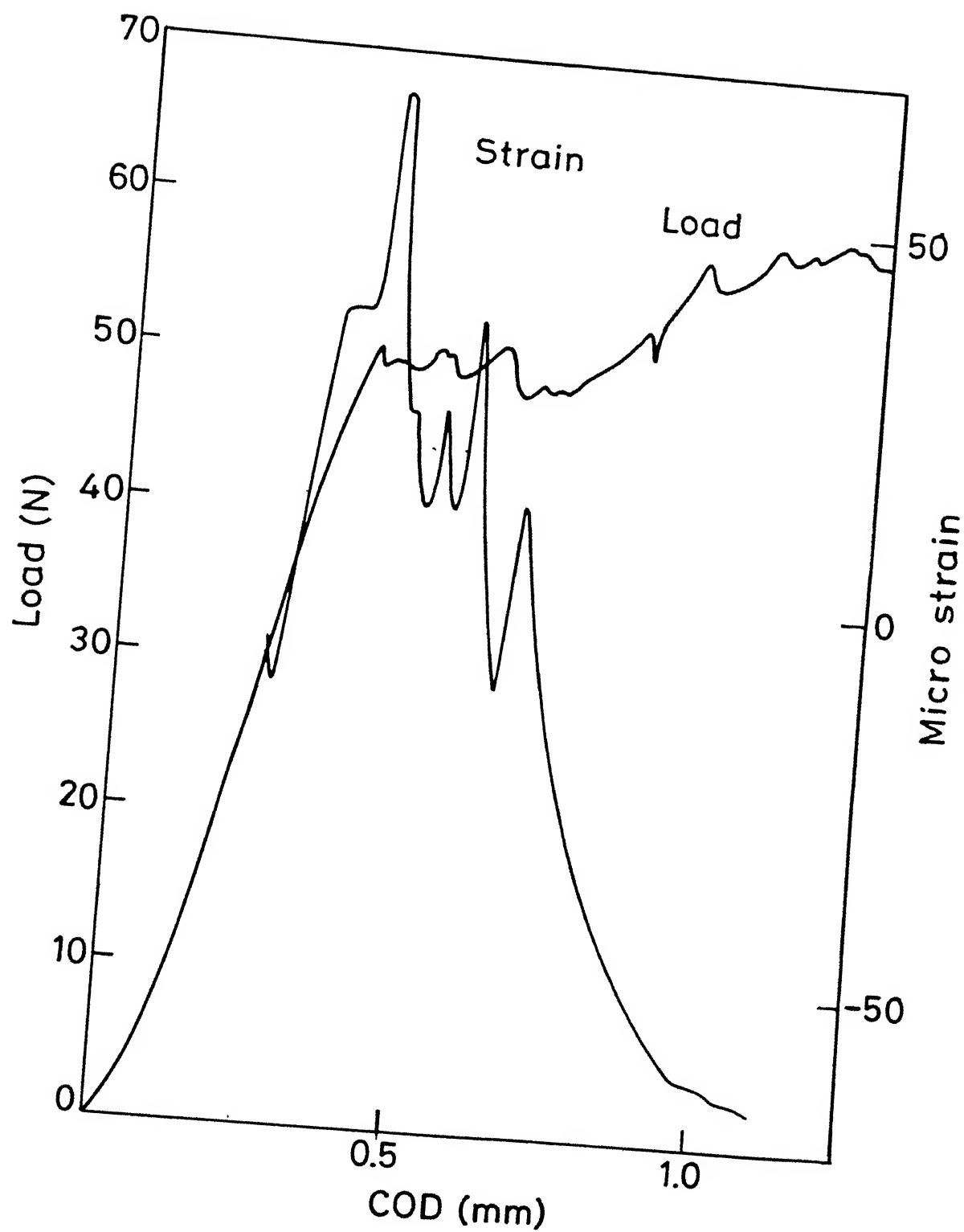Fig. 4.1 Experimentally Recorded Strain and Load for
Expt. No. 1.

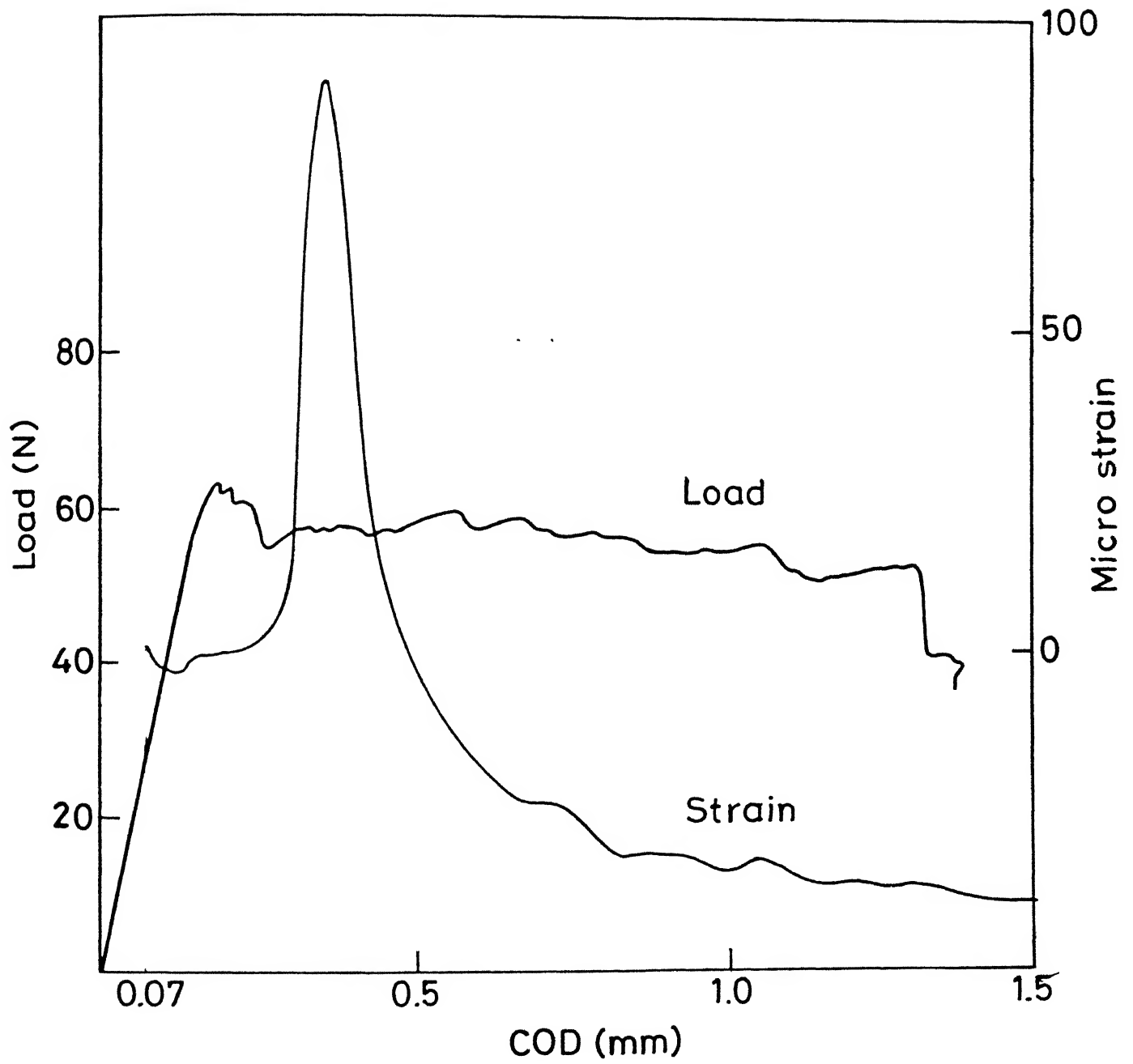Fig. 4.2 Experimentally Recorded Strain and Load for Expt. No. 2.

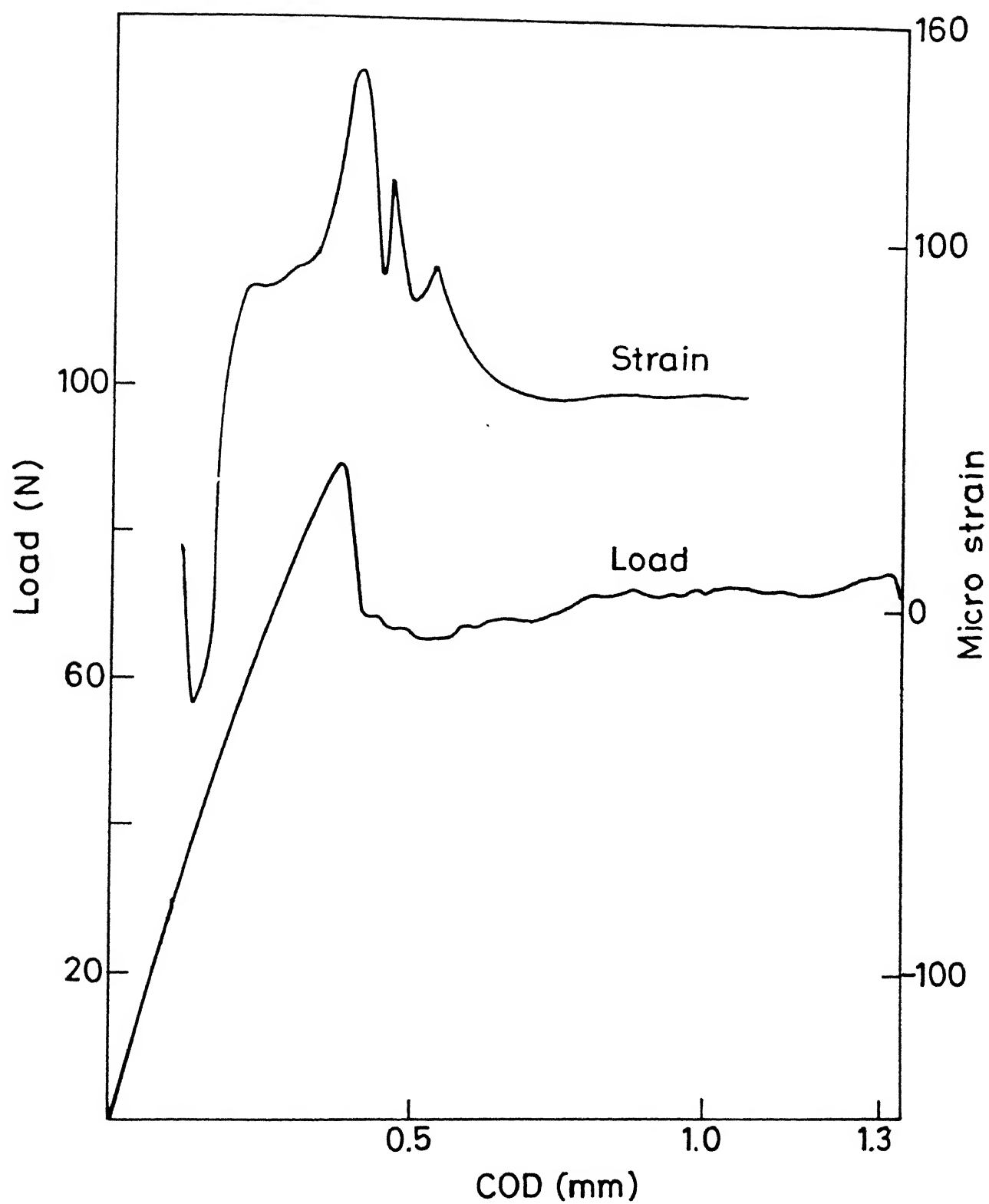Fig. 4.3 Experimentally Recorded Strain and Load for
Expt. No. 3.

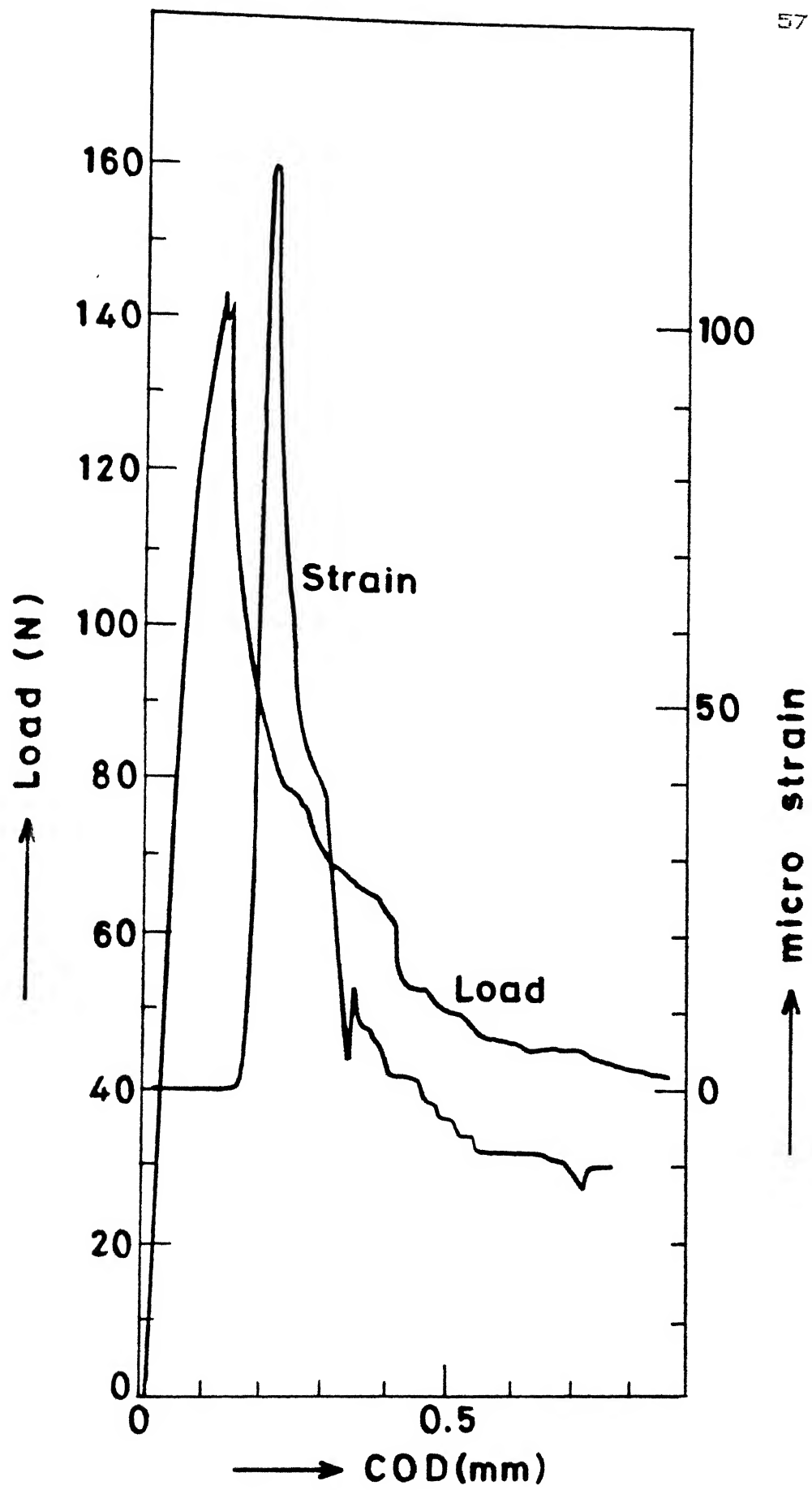Fig. 4.4   Experimentally Recorded Strain and Load for
Expt. No. 4.

Fig. 4.5 Experimentally Recorded Strain and Load for Expt. No. 5.
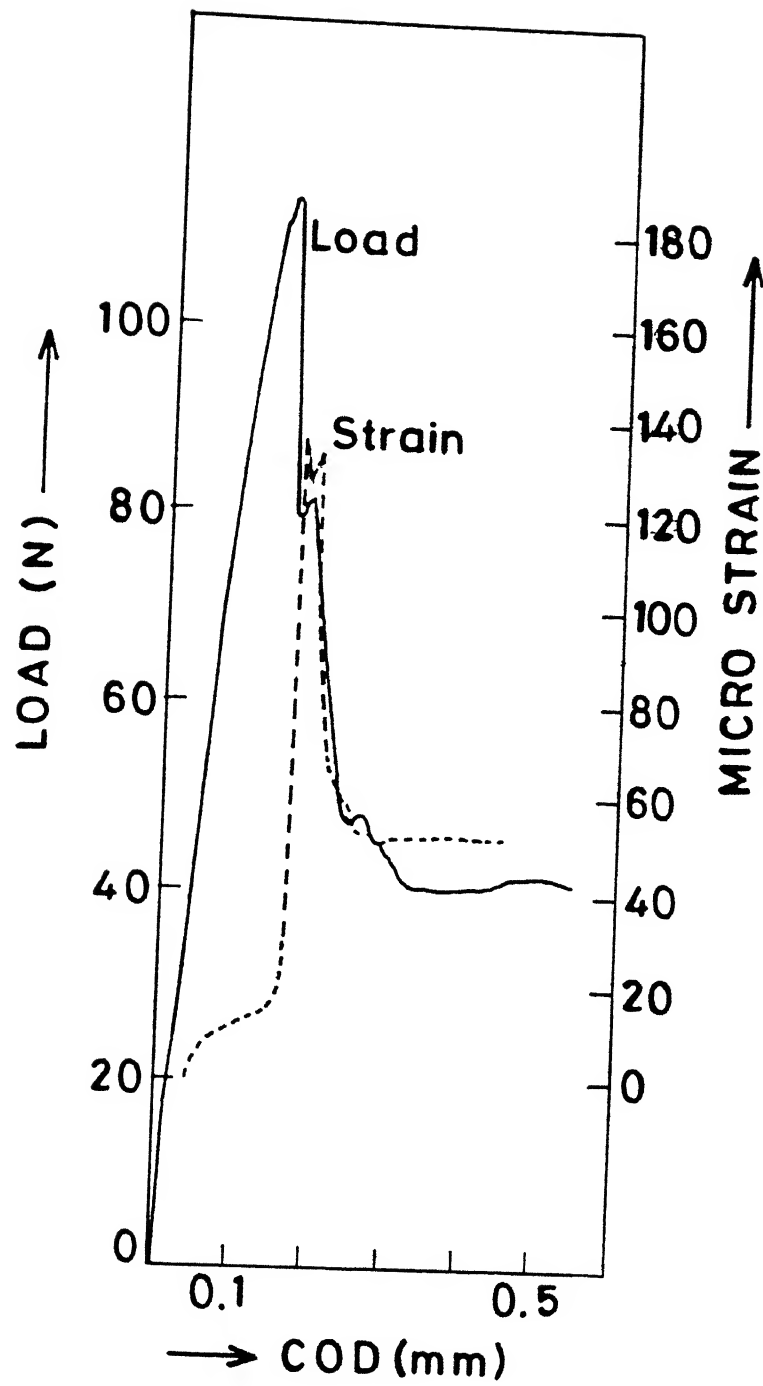
Fig. 4.6 Experimentally Recorded Strain and Load for Expt. No. 6.

CHAPTER V

CONCLUSIONS AND SUGGESTIONS FOR FUTURE WORK

The aim of the work has been to experimentally determine the stress intensity factor by measuring strain near crack tip through a strain gauge in a double cantilever specimen with thin cantilevers. A finite element software has been developed for estimating the strain field which has been used in selecting a proper position and orientation for fixing a small strain gauge of 0.2mm.

The finite element code was validated by solving two standard problems. The software was then used to determine the stress intensity factor as well as the strain field for the DCB specimen having thin cantilevers. The numerical value of stress intensity factor is in good agreement with the one obtained through energy approach.

The DCB specimen has been made by bonding two thin strips of hardened alloy steel with epoxy. The curing was done at a temperature of 130° Celsius under a pressure of 1.2 MPa. While bonding, a precrack was introduced by keeping a BOPP sheet between the strips up to the required length. The strain gauge of gauge length 0.2 mm is bonded to the side face of the specimen at 45° with the help of a fixture made of self sticking paper.

The specimen is loaded in mode I in an INSTRON machine. The experiment is conducted quasi-statically under controlled displacement conditions. As the crack grows and approaches the strain gauge, the output from the strain gauge increases till it reaches a peak. The peak corresponds to the location of the crack tip at about 1.5 mm prior to the strain gauge measured along the crack plane. Further crack extension reduces the strain. The measured peak strain gives the value of critical stress intensity factor through the relationship between strain

and SIF which is obtained through the computer programme. This experimentally obtained value of K_{IC} has been compared with the numerical prediction calculated using the load corresponding to the instant at which strain reaches the peak value, with the help of the numerical programme.

The measured strains are found to be lower by 8 to 55 % than the values predicted by the finite element analysis. The reason is thought to be imperfect bonding between the cantilevers due to entrapped air bubbles. This affects the stress/strain field and make the analysis imperfect.

In future, bonding of the specimen may be done in a vacuum bag which will avoid air entrapment and give a better bond. The method can be extended to dynamic problems and composite materials.

APPENDIX A

The behaviour of quarter point element is explained below
[10]. The derivation is for 1-D and can be extended to higher
dimensions since the nodes on any sides of a rectangular element
are not affected by those on the other three sides.

An element having side nodes can be made to display a square
root singularity in stress or strain by suitably defining its
geometry. Consider for example the three noded bar element as
shown in Fig. A.1 (a).

The displacement u at any point is given as

$$u = N_1 u_1 + N_2 u_2 + N_3 u_3 \qquad \qquad \dots (A.1)$$

and the coordinate x at any point is

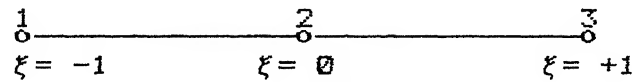$$x = N_1 x_1 + N_2 x_2 + N_9 x_3 \qquad \qquad \dots (A.2)$$
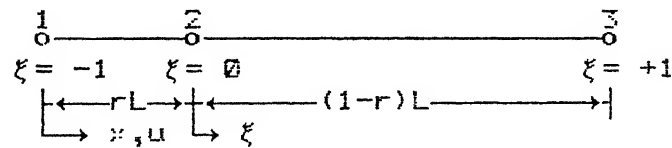

Figure A.1(a).

Figure A.1(b).

where N_ι s are the shape functions defined as

$$
\left.
\begin{aligned}
N_1 &= \tfrac{1}{2} \, \xi \, (1-\xi) \\
N_2 &= (1-\xi^2) \\
N_3 &= \tfrac{1}{2} \, \xi \, (1+\xi)
\end{aligned}
\right\} \qquad \dots (A.3)
$$

Substituting in Eq.A.2,

$$x = \frac{\xi}{2} (\xi-1)x_1 + (1-\xi^2)x_2 + \frac{\xi}{2} (1+\xi)x_3 \qquad \ldots (A.4)$$

If the third node is shifted to a point which is at a distance rL from node 1, it can be shown that $r = \frac{1}{4}$ for the stress to be singular at node 1 and that the nature of singularity is a square root one (Fig A.1.(b)). From the figure,

$$x_1 = 0, \quad x_2 = rL, \quad x_3 = L$$

Hence from equation A.4,

$$x = \frac{L}{2} \left[2 r - 2 r \xi^2 + \xi + \xi^2 \right] \qquad \ldots (A.5)$$

Now differentiating displacement u with respect to x,

$$\frac{\partial u}{\partial x} = \frac{\partial u}{\partial \xi} \frac{\partial \xi}{\partial x} = \left[\frac{\partial u}{\partial \xi} \right] [J]^{-1} \qquad \ldots (A.6)$$

where [J] denotes the Jacobian given by

$$J = \frac{\partial x}{\partial \xi} = \frac{L}{2} \left[- 4 r \xi + 1 + 2 \xi \right] \qquad \ldots (A.7)$$

Substituting in Eq.A.6,

$$\frac{\partial u}{\partial x} = \frac{\partial u}{\partial \xi} \left[\frac{L}{2} (-4 r \xi + 1 + 2 \xi) \right]^{-1} \qquad \ldots (A.8)$$

At node 1, $\xi = -1$ and $x = 0$. Therefore,

$$\left. \frac{\partial u}{\partial x} \right|_{\substack{\xi=-1 \\ x=0}} = \frac{\partial u}{\partial \xi} \left[\frac{L}{2} (4 r + 1 - 2) \right]^{-1} = \frac{\partial u}{\partial \xi} \left[\frac{L}{2} (4 r - 1) \right]$$

For $\quad \dfrac{\partial u}{\partial x}\Big|_{\zeta=-1} \longrightarrow \infty$,

$$\dfrac{L}{2}(\ 4\ r\ -\ 1\ )\ =\ 0\ \Rightarrow\ r\ =\ \dfrac{1}{4} \qquad \ldots (A.9)$$

Substituting in Eq.A.5,

$$x\ =\ \dfrac{L}{4}(\ 1\ +\ \zeta\ )^2$$

or, $\quad (\ 1\ +\ \zeta\ )\ =\ \sqrt{\dfrac{4\ x}{L}} \qquad \ldots (A.10)$

Substituting it in Eq.A.7 along with the value of r, J simplifies to

$$J\ =\ \dfrac{\partial x}{\partial \zeta}\ =\ \dfrac{L}{2}\ (\ 1\ +\ \zeta\ )$$

i.e., $J^{-1}\ =\ \dfrac{1}{L}\sqrt{\dfrac{L}{x}} \qquad \ldots (A.11)$

Using equations A.3, A.10 and A.11 in A.8, one obtains

$$\dfrac{\partial u}{\partial x}\ =\ \left[(\ \dfrac{2}{L}\ -\ \dfrac{3}{2L}\sqrt{\dfrac{L}{x}}\ )u_1\ -(\ \dfrac{4}{L}\ -\ \dfrac{2}{L}\ \sqrt{\dfrac{L}{x}}\ )u_2\ +(\ \dfrac{2}{L}\ -\ \dfrac{1}{2L}\ \sqrt{\dfrac{L}{x}}\ )u_3\right]=f\left(\dfrac{1}{\sqrt{x}}\right)$$

which means stress is inversely proportional to square root of the distance from the node.

APPENDIX B

Equation used in calculating K_I through G_I has been derived here. G can be calculated by the formula [8],

$$G = \frac{P^2}{2}\frac{\partial C}{B\partial a} \qquad \qquad \ldots (B.1)$$

where B is the thickness, a is the crack length and C is the compliance of the specimen and P is the applied load. C is defined as $C = \frac{u}{P}$ where u is the displacement of the point loads.

For a cantilever with length L, moment of inertia I and Young's modulus E under the action of a force P, $u = \frac{PL^3}{3EI}$. In the case of a DCB specimen, the length of each of the cantilevers is equal to the crack length and since there are two cantilevers,

$$C = \frac{2u}{P} = \frac{2 a^3}{3EI} \qquad \qquad \ldots (B.2)$$

Substituting Eq. B.2 in B.1, the expression for G is obtained as

$$G_1 = \frac{12 P^2 a^2}{2 B a^3} \qquad \qquad \ldots (B.3)$$

Using the relation $G_1 = \frac{K_1^2}{E}(1-\nu^2)$ for plane strain, the equation yields

$$K_1 = \frac{2\sqrt{3} P a}{B h^{3/2}(1-\nu^2)} \qquad \qquad \ldots (B.4)$$

REFERENCES

1. N. Takeda, R. L. Sierakowski, C. A. Ross & L. E. Malvern
   -Delamination Crack Propagation in Ballistically Impacted Glass/Epoxy Composite Laminates.
   -Experimental Mechanics, 22 (1982) pp 20-5

2. Prashant Kumar, D. K. Sarkar & S. C. Gupta
   -Rolling Resistance of Elastic Wheels on Flat Surfaces
   -wear, 126 (1988), pp 117-129

3. A. J. Rosakis, J. Duffy & L. B. Freund
   -The Determination of Dynamic Fracture Toughness of AISI 4340 steel by the shadow spot method.
   -Journal of Phys. solids, Vol. 32, No. 4 (1984), pp 443-60

4. A. Shukla, B. D. Agarwal & Bharat Bhushan
   -Determination of Stress Intensity Factor in Orthotropic Composite Materials using strain gauges.
   -Engineering Fracture Mechanics, Vol. 32, No. 3 (1989), pp 469-77

5. J. R. Berger & J. W. Dally
   -A Spacially Overdetermined Analysis for Propagation Poughness Using Strain Gauges.
   -Mechanical Research Communications, Vol 17 (2), pp 93-?

6. T. Nishioka, T. Murakami, H. Uchiyama, K. Sakakura & H. Kittaka
   -Specimen Size Effects on Dynamic Crack Propagation and Arrest in DCB Specimens.
   -Engineering Fracture Mechanics, Vol 39, No. 4 (1991), pp 757-767

7. O. Kolenik
   -On the Physical Meaning of the J-Δa Curves
   -Engineering Fracture Mechanics, Vol 38, No. 6 (1991), pp 403-412

8. David Broek
   -Elementary Engineering Fracture Mechanics.
   -Martinus Nijhoff Publishers.

9. R. D. Cook
   -Concepts and Applications of Finite Element Analysis.
   -John Wiley & Sons.

10. R. S. Barsowm
    -On the Use of Isoparametric Finite Elements in Linear Fracture Mechanics.
    -International Journal of Numerical Methods in Engineering, Vol. 10 (1976), pp 25-37

11. L. P. Harrop
   -The Optimum Size of Quarter-Point Crack-Tip Element.
   -*International Journal of Numerical Methods in Engineering,
   Vol. 17, pp 1101-3*

12. Dr. K. Ramesh, Department of Mechanical
   Engineering, I I T, Kanpur.

13. S. Q. zhang, B. Z. Jang, B. T. Valaire & J. C. Suhling
   -A New Criterion for Composite Material Mixed Mode Fracture
   Analysis.
   -*Engg. Fracture Mechanics, Vol 34, no. 3 (1989), pp 749-769*

14. E. P. Popov
   -Mechanics of Materials.
   -*2nd Edition, Prentice Hall,Inc.*

15. M. D. Narayanan
   -M. Tech Thesis (1988).